TRANSPORT, CORRELATION AND STRUCTURAL DEFECTS (pp. 27–61)
edited by Hellmut Fritzsche

PERSISTENT INFRARED SPECTRAL HOLE BURNING OF IMPURITY VIBRATIONAL MODES IN CHALCOGENIDE GLASSES

S. P. Love and A. J. Sievers
Laboratory of Atomic and Solid State Physics and Materials Science Center
Cornell University
Ithaca, New York 14853

ABSTRACT

Persistent infrared spectral hole burning of impurity vibrational modes is used to study host-defect dynamics in chalcogenide glasses, the first class of glassy systems to exhibit non-electronic persistent hole burning. New hole burning systems identified include the CO_2, D_2O, OD, and SH molecules in As_2S_3; CO_2 and SeH in amorphous Se; and SeH in As_2Se_3. Basic principles of persistent spectral hole burning are reviewed and details of applying the technique in the mid-infrared using lead-salt semiconductor diode lasers are discussed. Results for the various systems are consistent with local host restructuring as the hole burning mechanism, and show that the host determines both the non-exponential spontaneous hole filling and the temperature-dependent optical dephasing behaviors.

I. INTRODUCTION

Persistent spectral hole burning (PSHB) is a high-resolution laser spectroscopic technique which provides a means of probing the microscopic dynamics of a solid through its interactions with optically active impurity molecules. In essence, the technique uses a narrow bandwidth laser to selectively bleach the optical absorption arising from the small subset of impurities which happen to be in resonance with the laser frequency. The resulting reduction in absorption strength in the narrow frequency region about the laser frequency is known as a "spectral hole" and if the lifetime of this hole is longer than any of the impurity excited state lifetimes, the hole is said to be persistent. Persistent hole lifetimes at liquid helium temperatures typically range from a few seconds

to many hours or even days. The utility of the phenomenon lies in the fact that, because only those centers in resonance with the laser are involved in the hole burning, it is possible to extract the lifetime-limited homogeneous linewidth, which would ordinarily be obscured within the disorder-dominated inhomogeneous absorption band. Furthermore, because in glasses the hole burning process itself is intimately connected with the existence of multiple metastable configurations of the glass, it is possible, by studying the time evolution of the spectral hole, to learn about the low temperature relaxation dynamics among these glassy configurations.

Persistent spectral hole burning is to be contrasted with the older technique of transient saturation hole burning.[1,2] The latter is a high intensity technique, requiring that the rate at which photons are absorbed be comparable to the rate at which the impurities relax back to their ground state; intensities used are typically several kW/cm^2, and these holes persist only as long as the excited state lifetime, typically on the order of a nanosecond. In persistent spectral hole burning, high laser intensities are not required. The long lifetime of the effect makes it possible for a spectral hole to gradually build up over time, even at low intensity. Typical cw laser intensities for the work reported here range from a few mW/cm^2 to roughly 100 mW/cm^2.

The earliest instances of persistent spectral burning involved electronic transitions of organic dyes in amorphous organic matrices. These first observations were reported in 1974 by Gorokhovskii et al.[3] for free-base phthalocyanine in a frozen n-octane matrix, and by Kharlamov et al.[4] for perylene and 9-aminoacridine in glassy ethanol matrices. Since these initial discoveries, numerous other examples of systems exhibiting PSHB for impurity electronic transitions have been discovered both in other organic systems[5] and in inorganic systems such as rare earth ions in silicate glasses.[6] In the course of these discoveries, it became clear that there were several mechanisms by which PSHB could occur. These mechanisms tend to fall within two broad categories: photochemical hole burning (PHB), in which the laser induces a change in the electronic properties of the impurity molecule itself, breaking a bond for example, and non-photochemical hole burning (NPHB), in which the impurity molecule remains essentially unchanged but either it reorients or the host matrix around it changes. It is this latter type of hole burning which is will be of interest here.

All the early NPHB systems mentioned above involved electronic transitions of the impurity molecules, with photon energies on the order of 2 eV. This class of systems has continued to be a major focus of persistent hole burning studies, in part due to the availability of tunable dye lasers in the visible region. In view of the large perturbation associated with electronic excitation, however, it is unclear whether behavior probed using electronic spectral hole burning is representative of the unperturbed glass. It remained to be seen whether PSHB, and in particular NPHB, was possible for the much lower energy infrared transitions associated with excitation of impurity vibrational

modes, with all electronic degrees of freedom remaining in their ground state. The first examples of persistent infrared spectral hole (PIRSH) burning of impurity vibrational modes in solids[7] were reported in 1979 for matrix-isolated molecules in frozen noble gas Van der Waals matrices.[8–10] Soon after, PIRSH burning was discovered for vibrational modes of ionic impurities in alkali-halide crystals, beginning with the perrhenate ion[11–13] ReO_4^-, followed by the CN^-:Na^+ defect[14,15] and the NO_2^- ion.[16,17] Defect reorientation was identified as the mechanism for these PIRSH burning systems.

The discovery of PIRSH burning for the sulfur-hydrogen stretch mode in hydrogenated As_2S_3 glass demonstrated for the first time that vibrational hole burning was not restricted to ionic and Van der Waals solids, but could occur in covalently bonded glasses as well.[18,19] It was soon found[20] that the As_2S_3:SH system was not an anomaly, but rather the first in a broad class of systems. Several new host-impurity combinations, including D_2O, OD, and CO_2 in As_2S_3, SeH and CO_2 in glassy Se, and SeH in As_2Se_3, have been successfully prepared, and all exhibit PIRSH burning. So far, PIRSH burning appears to be a universal phenomenon in the chalcogenides.

A number of factors make impurity vibrational modes particularly well-suited for persistent hole burning studies of the chalcogenides. The first of these is the matter of finding an impurity which absorbs at a frequency where the host is transparent. Since persistent hole burning typically relies on absorptions due to dilute impurities, relatively thick samples, on the order of a few millimeters, are usually required to obtain the necessary absorption strength. It is thus imperative that the experiments be performed in a frequency region in which the host is transparent. The infrared-active vibrational modes of molecules made up of relatively light atoms have frequencies which fall nicely within the transparent window of the chalcogenides, between the bulk phonon and the electronic band gap absorptions.

A second consideration is the ease with which the impurity can be introduced into the host. An impurity with absorption at the right frequency is, after all, of no use if it is insoluble in the host material. In this respect, the small, light molecules used here again appear to be ideal. It was recognized as early as 1953 that exposing molten chalcogenides to air could lead to new IR absorptions in the melt-quenched glass, although at that time the species present in the glass were not identified.[21] Thus common atmospheric gases were obvious candidates for producing hole burning defects. It has been found that many of these molecules, such as CO_2 and water, go into chalcogenide glasses so easily, and exist in the atmosphere in such large concentrations, that it is very difficult to produce a sample *without* these impurities. Since chalcogenide glasses are emerging as important materials for IR optical fiber applications, a better understanding of the dynamics of these common defects is also desirable from a purely technological viewpoint.

Finally , because the chalcogenides are good glass formers over such a wide range of alloy compositions, they offer a promising system for attacking the general problem of

persistent hole burning in glasses. The discovery of PIRSH burning in this system presents the possibility of systematically determining correlations between the hole burning behavior and other composition-determined properties of the glass. This work is still in its very early stages, but it will be seen that substantial variations in hole burning behavior do exist within the chalcogenide system.

The organization of this chapter is as follows. In section II, a review of the basic principles of persistent spectral hole burning is provided. Section III discusses the details of the experiments and section IV presents the results of the experiments. Finally, section V provides a discussion of the results and prospects for future experiments. Throughout this article, we shall follow the spectroscopists' convention of referring to all energies and frequencies in terms of the reduced frequency or wavenumber, given in cm^{-1}. For those unfamiliar with this convention, the wavenumber is defined as the reciprocal of the wavelength (without any factor of 2π), or equivalently, as the frequency divided by the speed of light; thus 1 cm^{-1} equals 30 GHz, and 1 eV equals 8066 cm^{-1}.

II. BASIC CONCEPTS OF PERSISTENT SPECTRAL HOLE BURNING

In order to understand persistent spectral hole burning and the information it can provide, it is first necessary to review the factors which contribute to the optical lineshapes for defects in solids.[22] First consider an ensemble of identical molecules experiencing identical local environments. An incident electromagnetic wave will set up a coherent superposition of the ground and excited states of these impurity molecules, with an associated oscillating dipole moment. The sum over all the impurities thus gives rise to an oscillating macroscopic polarization whose lifetime determines the width of the absorption line for this ensemble. This lifetime is governed by the rate at which the phase coherence among the individual molecules is lost, and hence is known as the dephasing time, usually denoted T_2. Two contributions determine the dephasing rate $1/T_2$. The first comes from the decay rates of the two states involved; since we will be dealing with the situation where the lower state is the ground state, with essentially infinite lifetime, only the excited state lifetime T_1 will appear. The second contribution comes from processes which interrupt the phase of the individual molecules, destroying the phase coherence and hence the macroscopic polarization, without altering the population of the energy levels. These are known as pure dephasing processes, and their characteristic time is denoted T_2^*. The total dephasing rate is given by

$$\frac{1}{T_2} = \frac{1}{2T_1} + \frac{1}{T_2^*} \tag{1}$$

and the resulting Lorentzian absorption line has a width γ_h given by

$$\gamma_h = 1 / \pi T_2 \tag{2}$$

known as the homogeneous width.

The mechanisms for the pure dephasing contributions T_2^* depend on the system being studied. A familiar example is collisional dephasing in gaseous systems, the source of so-called "pressure broadening." In crystalline solids, the dominant dephasing process is the scattering of phonons from the impurity. In the case of amorphous solids, the situation is more complicated, and not as well understood. The most generally accepted models for impurity optical dephasing in glasses at low temperatures involve the so-called "two-level systems" (TLS) originally proposed to explain the anomalous low temperature specific heat of glasses.[23,24] This will be discussed further in Section V. The important point is that in solids, homogeneous lineshapes convey information about the dynamics of the host-defect system, with the defect acting as a microscopic probe of the host excitations.

The situation is not quite so simple in real solids, however, particularly in amorphous solids, because the defects in general do *not* experience identical local environments. As shown schematically in Fig. 1, differences from site to site in the way

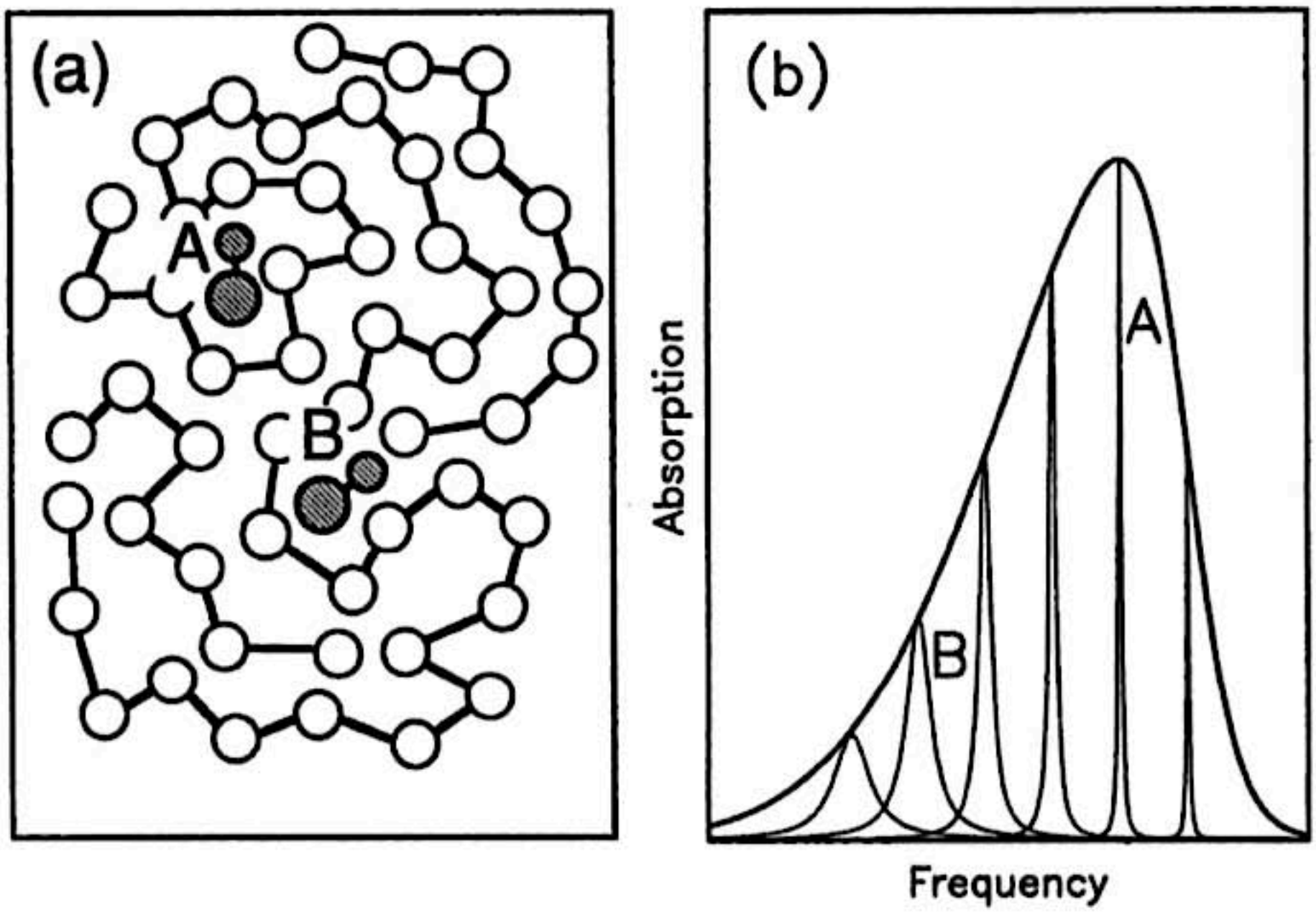

Fig. 1 Inhomogeneous Broadening. (a) Two impurity molecules, labelled "A" and "B", with different local environments in an amorphous host give rise to homogeneous infrared absorption lines with corresponding labels in (b). The broad envelope in (b), the sum over all impurities, is the observed inhomogeneous absorption band.

the host couples to the impurity energy levels lead to different absorption frequencies for each molecule. In addition, these differences in coupling can result in variations in the homogeneous width at the various kinds of site. Thus, if one could look at only those defects identical to the one labelled "A" in Fig. 1(a), the homogeneous absorption line labelled "A" in Fig. 1(b) would be observed. Likewise, defect "B", whose environment is substantially different from that of "A", would give rise to a homogeneous band with a different center frequency and width. What is actually observed in linear absorption spectroscopy, of course, is the sum over the entire distribution of possible environments, resulting in an absorption band many times wider (in glasses, typically by a factor of 10^3 to 10^5) than the homogeneous widths determined by dephasing rates. This is known as inhomogeneous broadening. In an inhomogeneously broadened system, the optical lineshapes obtained by linear spectroscopy no longer convey dynamical information.

Persistent spectral hole burning provides, for suitable systems, a means of recovering this dynamical information. The basic requirements for producing persistent spectral changes are that there exist at least two stable quasi-ground state configurations for the host-defect system, that relaxation between these "ground states" occurs on a much slower time scale than the defect excited state lifetimes, and that there exists an optical pumping pathway, involving an excited state of the defect, connecting the two ground states. The basic process for PSHB is illustrated for the general case in Fig. 2. In Fig. 2 (a), the host-defect system is represented in a configuration coordinate diagram, with the total energy of the system plotted as a function of the generalized configuration coordinate q, the lower curve corresponding to the defect in its ground state, the upper curve to the defect in its excited state. The system is initially in the stable configuration represented by the left well of the double-well potential. For those defects whose environments produce the proper energy level spacing in the impurity, the transition to the excited state can be made by absorption of a laser photon of energy $\hbar\omega_L$ (solid arrow in Fig. 2). After most absorption events, the defect simply relaxes back to its original ground state, with the system remaining in the left-hand well. But there exists a finite probability that from the defect's excited state, the system can undergo a configuration change to the right-hand well, indicated by the dashed arrow in Fig. 2. The probability that for a given absorption event the configuration change will occur is known as the quantum efficiency for the hole burning process. With the system in the new configuration, the impurity's energy level spacing is changed and its absorption no longer lies at the laser frequency. Thus, at temperatures sufficiently low that thermal activation over the barrier is negligible, and with tunneling between the wells sufficiently slow, centers absorbing at the laser frequency will gradually be removed from the left-hand well and trapped in the other configuration, thus reducing the number of centers absorbing at that frequency. The result, shown in Fig. 2 (b), is a reduction in absorption strength, i.e. a spectral hole, centered at the laser frequency.

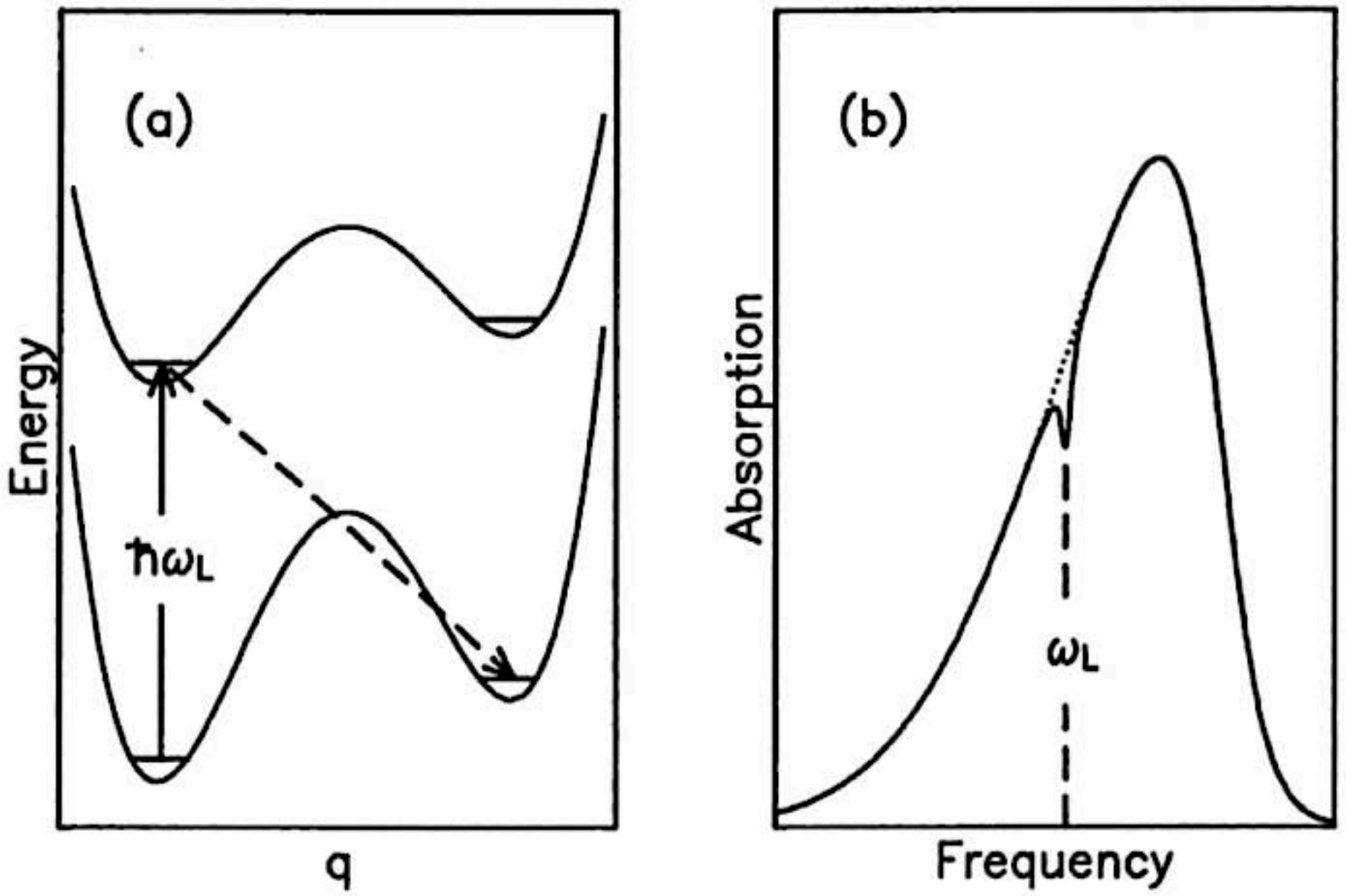

Fig. 2 General mechanism for persistent spectral hole burning. (a) Configuration coordinate diagram for a host-defect system having two metastable configurations. The two curves represent the system with the defect in its ground and excited states. A laser of energy $\hbar\omega_L$ excites defects in resonance with it (solid arrow); from the excited state, there exists a finite probability that the system will relax to the other configuration (dashed arrow), resulting in (b) a spectral hole at the laser frequency.

The general configuration coordinate q may represent any of several things, depending on the system. Persistent spectral hole burning in various systems has been attributed to the following mechanisms: (1) ionization of the defect with subsequent trapping of the electron,[25,26] in which case q is the electron coordinate and the two wells represent the defect and the trap; (2) internal rearrangement of the bonds in the defect molecule,[27] so that q again is an electron coordinate, but the wells represent the different bonding configurations; (3) reorientation of the defect with respect to the host,[7] in which case q is the angle of rotation of the defect; (4) rearrangement of local host structure around the defect, in which case q is a generalized configuration coordinate describing the positions of the glass atoms involved. These mechanisms have traditionally been divided into two broad classes: Mechanisms (1) and (2) are examples of photochemical hole burning (PHB), in which laser radiation changes the electronic structure of the impurity molecule itself, typically resulting in a photoproduct molecule with optical absorptions far removed from the original frequency, outside the original inhomogeneous band. The other two mechanisms are examples of non-photochemical hole burning (NPHB), in which the impurity molecule remains intact, and absorption is lost from the laser

frequency through changes in the interactions between defect and host. A hallmark of this latter type of hole burning is the much smaller range of the redistribution of absorption strength; the hole-burned centers have their frequency shifted by only a small amount, so that the absorption strength lost from the hole is relocated nearby, inside the original inhomogeneous band. These two classes of mechanisms, however, are not absolutely distinct and systems with intermediate behavior exist, such as the CN^-:Na^+ defect in KBr, whose reorientational mechanism would ordinarily be considered NPHB, but whose spectral signature suggests PHB.[14,15]

We now need to relate the shape of the spectral hole to the homogeneous line shape. To simplify the discussion, let us assume that all defects have the same homogeneous width and that all defects may be hole-burned with the same quantum efficiency. Let the absorption due to each defect be described by a frequency-dependent absorption cross section $\sigma_c(\omega)$ given by

$$\sigma_c(\omega) = \sigma_0\, g(\omega - \omega_c) \tag{3}$$

where σ_0 is a constant with dimensions of area times frequency, assumed here to be the same for all centers, and $g(\omega - \omega_c)$ is a normalized Lorentzian lineshape function centered at the frequency ω_c and having a width γ_h equal to homogeneous linewidth:

$$g(\omega - \omega_c) = \frac{\gamma_h/2\pi}{(\omega - \omega_c)^2 + (\gamma_h/2)^2} \tag{4}$$

The laser line is ordinarily narrow enough that it may be treated as a δ-function, so that its intensity per unit frequency may be written as

$$\frac{dI(\omega)}{d\omega} = I_0\, \delta(\omega - \omega_L). \tag{5}$$

For simplicity we shall assume that centers which undergo the hole burning configuration change are moved far enough away in frequency that we may ignore any absorption arising from them. With these approximations, we may write the following equation for the rate of change of the population of centers having center frequency ω_c:

$$\frac{dN(\omega_c)}{dt} = -[\, N(\omega_c) - N_B(\omega_c)]\frac{I_0 \eta \sigma_0}{\hbar\omega_L} g(\omega_L - \omega_c) + N_B(\omega_c)\Gamma_{BU} \tag{6}$$

Here $N(\omega_c)$ describes the inhomogeneous distribution and is defined so that $N(\omega_c)d\omega_c$ is the number of defects per unit volume with center frequency between ω_c and $\omega_c + d\omega_c$. $N_B(\omega_c)$ is the number of these converted to the hole-burned state, η the hole burning quantum efficiency, assumed to be the same for all centers which can be hole-burned, and Γ_{BU} is the rate of spontaneous relaxation from the burned to the unburned ground state configuration. In the limit of low laser intensity and short times, we may neglect the second two terms in Eq. (6), so that the change in $N(\omega_c)$ after time δt may be approximated by

$$\delta N(\omega_c) \approx - N(\omega_c) \frac{I_0 \eta \sigma_0}{\hbar \omega_L} g(\omega_L - \omega_c)\, \delta t \tag{7}$$

The resulting change in the absorption coefficient $\alpha(\omega)$ is obtained by multiplying this change in the density of absorbers by their absorption cross-section and integrating over all center frequencies:

$$\delta\alpha(\omega) = \int_0^\infty \delta N(\omega_c)\sigma_0 g(\omega - \omega_c)\, d\omega_c \tag{8}$$

If we assume that the width of the inhomogeneous distribution is much greater than the homogeneous width, an excellent approximation for glasses, then we may treat $N(\omega_c)$ as a constant, $N(\omega_L)$, and move it outside the integral. In this limit, we then have

$$\delta\alpha(\omega) \approx - N(\omega_L)\, \delta t \frac{I_0 \eta \sigma_0^2}{\hbar \omega_L} \int_{-\infty}^{\infty} g(\omega_L - \omega_c)\, g(\omega - \omega_c)\, d\omega_c, \tag{9}$$

where, since $\omega_c >> \gamma_h$, it is permissible to extend the lower limit of integration to negative infinity. The integral in Eq. (9) is the convolution of two identical Lorentzians, which, as can easily be shown, is itself a Lorentzian having twice the width of the original. We thus have the well known result that, for Lorentzian homogeneous lines, the hole in the short burn time, low intensity limit is a Lorentzian with a width equal to twice the homogeneous width, centered at the laser frequency:

$$\delta\alpha(\omega) = -\, N(\omega_L)\, \delta t\, \frac{I_0 \eta \sigma_0^2}{\hbar\omega_L}\, \frac{\gamma_h/\pi}{(\omega-\omega_L)^2+\gamma_h^2} \tag{10}$$

Under ideal conditions, then, the homogeneous linewidth may be determined from the hole width. We must now consider some of the complications which might invalidate Eq. 10. The first of these arises when we leave the small hole limit. Recall that the assumption of short burn times and low intensities, hence small holes, allowed us to neglect the second two terms of Eq. 6. It should be clear from inspection of Eq. 6 that these terms act to reduce the rate of hole burning and eventually lead to a steady state in which $N(\omega_c)$ no longer changes. Since the second term of Eq. 6 contains the lineshape factor $g(\omega_L - \omega_c)$, the hole growth saturation due to this term will first become apparent at the center of the hole, while the wings of the hole continue to grow. The result is a non-Lorentzian hole with the peak suppressed relative to the wings, thus having an apparent width greater than in the small hole limit. The spontaneous hole relaxation arising from the third term in Eq. 6 is spread evenly over the hole, and so tends to ameliorate to some extent the hole broadening due to the second term. Numerical calculations of the hole shapes in various regimes can be found in Ref.[28]. The practical implication of these effects is that in order to obtain homogeneous widths from hole widths, one must make certain that hole widths are measured in the small hole limit. This is perhaps best ensured by experimentally determining the hole width as a function of depth and then extrapolating to zero hole depth.[29]

A second process which can lead to broadened holes in amorphous systems is known as spectral diffusion. While the first complication was merely a matter of properly performing and interpreting the hole burning experiment, this second one arises from the essential physics of the amorphous state. Since glasses are, by their very nature, in a non-equilibrium state, their structure will continue to evolve with time even at low temperatures. If the evolution of local environments occurs on a sufficiently rapid time scale, impurity centers initially out of resonance with the burning laser may drift into resonance, undergo hole burning, and continue drifting in absorption frequency until the hole is probed. The result is a broadened hole which continues to broaden with time after burning ceases. Several examples of this type of behavior have been observed, and detailed studies may yield new insights into glassy dynamics.[30] The extent to which spectral diffusion occurs, however, varies widely from system to system, and it is not always observable. Thus while in some systems homogeneous widths obtained from persistent hole burning are considerably greater than those obtained by other methods, such as a photon echo experiment,[31] in other systems good agreement with other techniques is obtained.[29] It is therefore important to consider the possibility of spectral diffusion on the time scale of one's experiment before equating the hole width with twice

the homogeneous linewidth. Though not always practical, the definitive test of whether the hole width is revealing the true homogeneous width would be to perform a complimentary measurement, using a different technique, to independently determine the homogeneous width. Although no such test has yet been performed for the chalcogenide systems discussed here, hole widths have been carefully monitored over timescales ranging from 1 second to 10^4 seconds and no evidence of hole broadening by spectral diffusion has been observed in any of these systems. It thus seems likely that the hole widths in these systems are indeed indicative of the homogeneous widths.

III. EXPERIMENTAL DETAILS

Sample Preparation

The samples used in these studies are ingots of bulk melt-quenched As_2S_3, As_2Se_3, or Se glass. The molecular impurities necessary for persistent spectral hole burning are introduced into the glass samples by melting the glass in a sealed quartz tube containing roughly 650 torr of the gas-phase dopant. Dopants which have been found to produce strong infrared absorptions in the desired frequency region include carbon dioxide, hydrogen, which reacts with the chalcogenide glass to form SH or SeH defects, and D_2O. The sample tubes have volumes of roughly 20 cm^3 and contain about 1 cm^3 of glass starting material. Samples are heated well above the glass transition temperature, typically to about 500° C, and rocked continuously for 30 minutes to ensure reasonably uniform dispersion of the impurity throughout the sample. As_2S_3 and As_2Se_3 samples are air quenched at room temperature. Because of their tendency to devitrify, elemental Se samples are quenched more rapidly. It has been found that quenching rates sufficient to prevent crystallization, but not so rapid that thermal stresses crack the sample, can be achieved by alternatingly immersing the quartz tube in liquid nitrogen and exposing it to room temperature air. After determining that they are reasonably free of bubbles, either by direct visual inspection or using an near-IR imaging device, the quenched samples are then cut and polished. Samples in their final form are typically 3 to 10 mm thick.

Persistent Spectral Hole Burning Experiments

The experimental setup for persistent spectral hole burning is illustrated in Fig. 3. The sample is mounted in an optical access superfluid helium immersion cryostat (Janis super vari-temp) equipped with ZnSe inner windows and NaCl outer windows. The sample temperature, which can be varied continuously down to 1.5 K, is determined using a calibrated 1kΩ carbon resistor attached to the sample.

PIRSH burning experiments are performed using tunable Pb-salt diode lasers. The

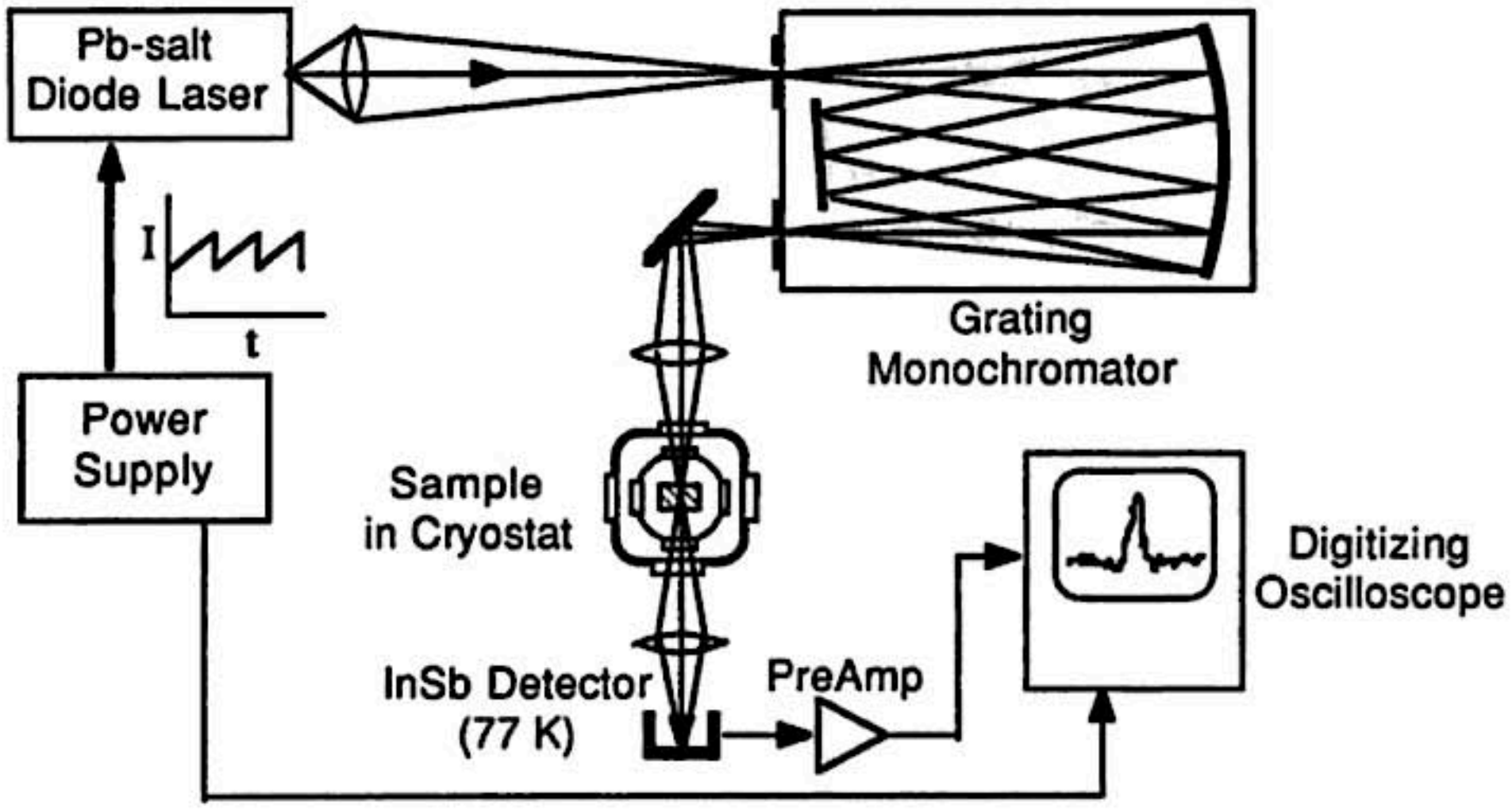

Fig. 3 Experimental Setup for PIRSH burning. See text for details.

diode lasers are mounted in a closed-cycle helium refrigerator as part of a commercially available system (Spectra-Physics). Typical output power for these lasers ranges from 10 to 100 μW, which, when focused to a small spot at the sample, can yield intensities up to several hundred mW/cm^2. Each individual diode can be coarsely tuned over a range of roughly 100 cm^{-1} by varying its operating temperature, which typically lies between 20 K and 80 K. The laser can be continuously tuned over a 1 - 2 cm^{-1} wide region by varying the current supplied to the diode. By applying a linear sawtooth modulation to the input current, the laser frequency can be repeatedly swept through the desired values at rates of roughly 1kHz. The output from the liquid nitrogen cooled InSb photovoltaic detector can thus be displayed on an oscilloscope, permitting changes in the infrared spectrum over this 1 - 2 cm^{-1} wide region to be observed essentially in real time. This rapid scanning over a relatively broad frequency region represents a considerable speed advantage over the tunable dye laser systems typically employed for hole burning studies in the visible, permitting observation of the time evolution of PIRSHs on time scales less than one second.

Oscilloscope traces from a typical PIRSH burning experiment are shown in Fig. 4 (a). These are obtained using a waveform digitizer (Tektronix 7D20) which allows up to 256 scans to be averaged for significant signal to noise improvement, and makes waveforms easily accessible for computer analysis. The lower trace in Fig. 4 (a) is a reference taken before burning any holes, and shows oscillations which merely reflect highly reproducible variations in laser output as a function of input current; all real

absorption features in this example are much too broad to produce significant signal variation across the narrow frequency range scanned here. After obtaining this reference scan, a spectral hole is burned by holding the laser current, and hence its output frequency, at a fixed value for a period of time, typically a few seconds to several minutes, depending on the nature of the experiment. The resulting persistent spectral changes are then probed by again scanning the laser frequency over a region centered on the burn frequency, as shown by the upper trace in Fig. 4 (a). If necessary, metal film neutral density attenuators may be inserted into the beam before the sample during probing to minimize the production of additional spectral modifications. A germanium etalon, which produces interference fringes of known frequency spacing, is used to calibrate the amplitude of the laser frequency sweep and thus determine the width of the observed spectral features. An oscilloscope trace taken with the etalon in the beam is shown in Fig. 4 (b). The absolute frequency is determined using a grating monochromator. The monochromator, which is placed between the laser and the sample, also serves to select a single laser mode out of the typically multi-mode diode laser output.

One final piece of information is needed to calculate the calibrated final result shown

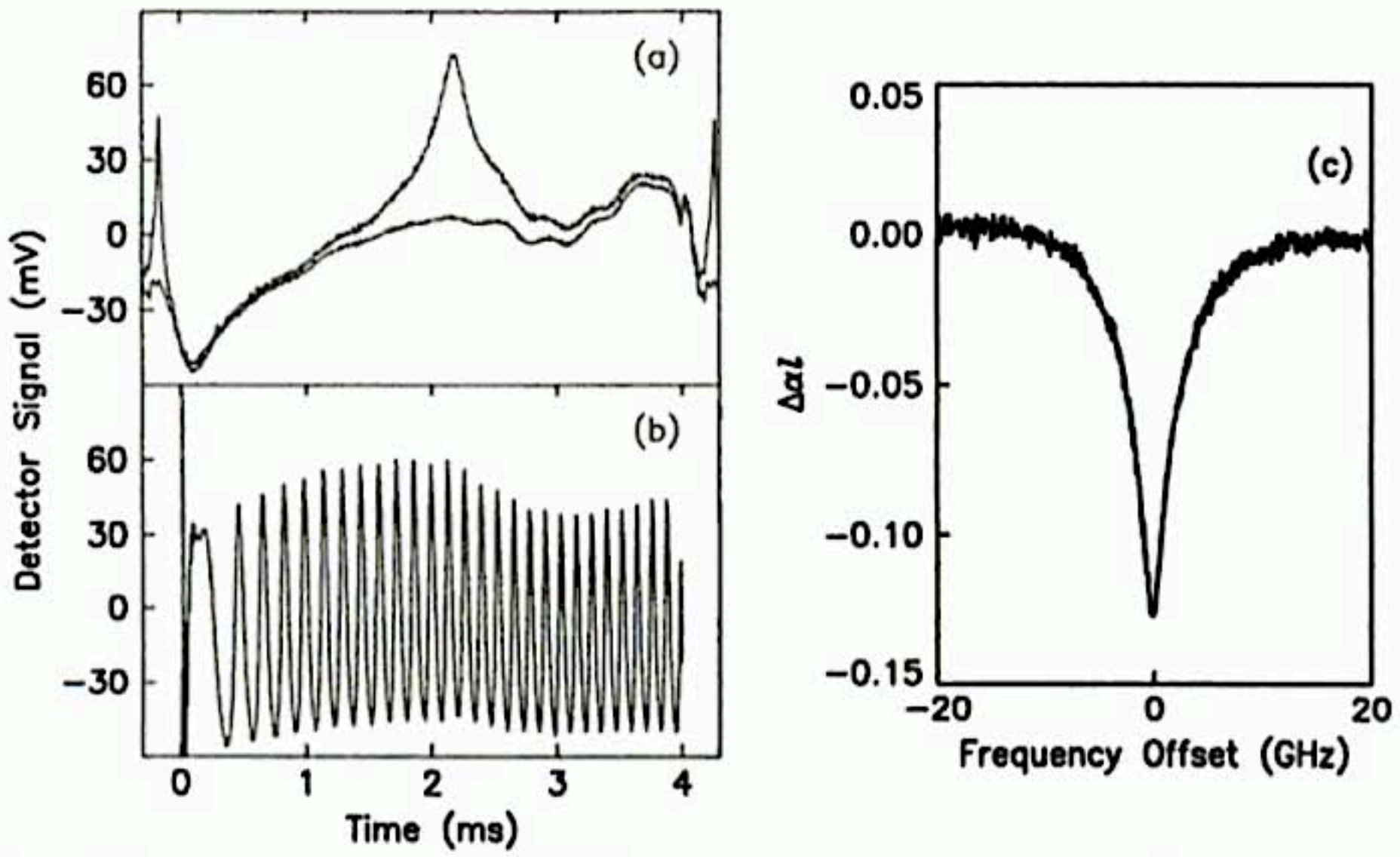

Fig. 4 Results from a typical PIRSH burning experiment. (a) Oscilloscope traces obtained before (lower trace) and after (upper trace) hole burning. (b) Oscilloscope trace taken with etalon in beam for frequency calibration. Laser frequency sweep amplitude is the same as in (a). Fringe spacing is 1.42 GHz. (c) Change in sample absorbance as a function of offset from burn frequency, calculated from the information in (a) and (b). The system for this example is As_2S_3:SH at 28 K, burned at 2503 cm^{-1}.

in Fig. 4 (c). Since a.c. coupling of the detector output to the oscilloscope is used, the large background signal from the unmodified sample transmittance is effectively subtracted off, allowing the small changes in signal amplitude resulting from PIRSH burning to be observed against an essentially zero baseline. In order to calculate the absolute magnitude of the spectral changes, the size of the background contribution must first be determined. This is easily accomplished by chopping the beam, thus defining the zero transmittance baseline. The laser induced changes in the absorption coefficient $\Delta\alpha$, shown in Fig. 4 (c), are then calculated using

$$\Delta\alpha l = -\ln (T_f / T_i) \tag{11}$$

where l is the sample thickness, and T_f and T_i are the final and initial transmitted intensities shown in the upper and lower traces of Fig. 4 (a), with the background contribution added on.

The technology of tunable Pb-salt diode lasers is still quite new, and though they can produce excellent results, one should be aware of the pitfalls associated with these devices. The first of these arises from the multimode output produced by virtually all of these lasers. Usually the laser output consists of several modes well separated in frequency, typically by 1 cm^{-1} or more, so that all but one mode may be eliminated using a grating monochromator. But occasionally two or more modes may be spaced by 1 GHz or less and cannot be separated by a monochromator. This results in anomalous satellite holes if the mode spacing is greater than the hole width, or in artificially broadened holes if the spacing is less than the hole width. The latter case is particularly insidious since it is often difficult to recognize in the hole spectrum. The same etalon used for frequency calibration serves as an important diagnostic tool for determining the quality of the diode laser output; non-sinusoidal fringes or beats in the fringe pattern are sure signs that multiple frequencies are present. It is occasionally possible, if absorption frequencies overlap, to utilize spectral hole burning in a well-studied system to diagnose the laser to be used in studying a new system. Various crystalline materials known to produce very narrow holes, for example, were used to verify that the surprisingly large hole widths seen for the SeH defect (see Sec. IV) are in fact real and not artifacts produced by multiple laser modes.

Another common problem encountered with these lasers is that the characteristic intensity variations, such as seen in Fig. 4 (a), though usually very reproducible, may sometimes vary on time scales of a few minutes. This introduces systematic baseline errors which cannot be divided out and hence obscure the true hole shape. This problem can be minimized by using samples having larger αl, so that the absolute size of the spectral holes is made greater for a given relative change in α, while at the same time the sample attenuates this systematic laser "noise." This solution is limited, of course, by the

fact that the sample also attenuates the total signal reaching the detector, so that a compromise must be made between attenuating the laser noise and keeping the total signal above the noise from other sources.

Finally, it should be noted that these semiconductor diode lasers are extremely prone to feedback instabilities[32] induced by light reflected back into the laser from surfaces anywhere in the experimental setup. Chaotic output fluctuations may occur even when extremely small fractions of the output power reenter the laser. For example, in one instance feedback problems were traced to a reflection from the detector window; hence, by the time the offending light reentered the diode, it had been attenuated by a factor of forty or so on its first pass through the sample and cryostat windows, and by the same amount on its return trip, in addition to the losses associated with the monochromator and various lenses. Feedback problems may usually be eliminated by ensuring that all optical elements, including windows, monochromator slits, and the sample itself, are tilted in such a way that light is not reflected back into the diode.

IV. RESULTS

Linear Spectroscopy.

An appropriate place to begin a discussion of persistent spectral hole burning is with a description of the simple linear spectra of the inhomogeneous absorption bands involved. The infrared spectra described here were obtained using a Fourier transform interferometer operating at a resolution of 0.5 cm^{-1}. Examination of these infrared spectra usually allows unambiguous identification of the impurities introduced in the doping process, and provides some information on the interactions between the host and impurity. Key features of the infrared spectra are summarized in Table 1.

Figure 5 shows the infrared absorption spectra for two glasses, glassy Se and As_2S_3, which have been treated in CO_2 gas as described in section III. The most prominent feature produced by the doping, a band with full width at half maximum (FWHM) of 6 cm^{-1}, centered at 2323.2 cm^{-1} in As_2S_3 and at 2321 cm^{-1} in Se, falls in the correct frequency range for the asymmetric stretching vibration (usually denoted ν_3) of the CO_2 molecule. For gaseous CO_2, the band origin lies at[33] 2349.146 cm^{-1}, so the host interaction produces roughly a 1% decrease in the frequency of this mode. Examination of the two additional weak absorption features, shown in Fig. 5 (c), leaves little doubt as to the assignment of these bands to the CO_2 molecule. These two lines, at 2258 cm^{-1} and 2306.5 cm^{-1} in As_2S_3, have the correct strengths, relative to the main 2323.2 cm^{-1} band, to be due to the isotopic species $^{13}C^{16}O_2$ and $^{18}O^{12}C^{16}O$ respectively. It is a simple matter to solve the equations of motion for a mass and spring model for the linear triatomic O-C-O molecule to obtain the normal mode frequencies. After first obtaining the spring constant from the $^{12}C^{16}O_2$ asymmetric stretch frequency

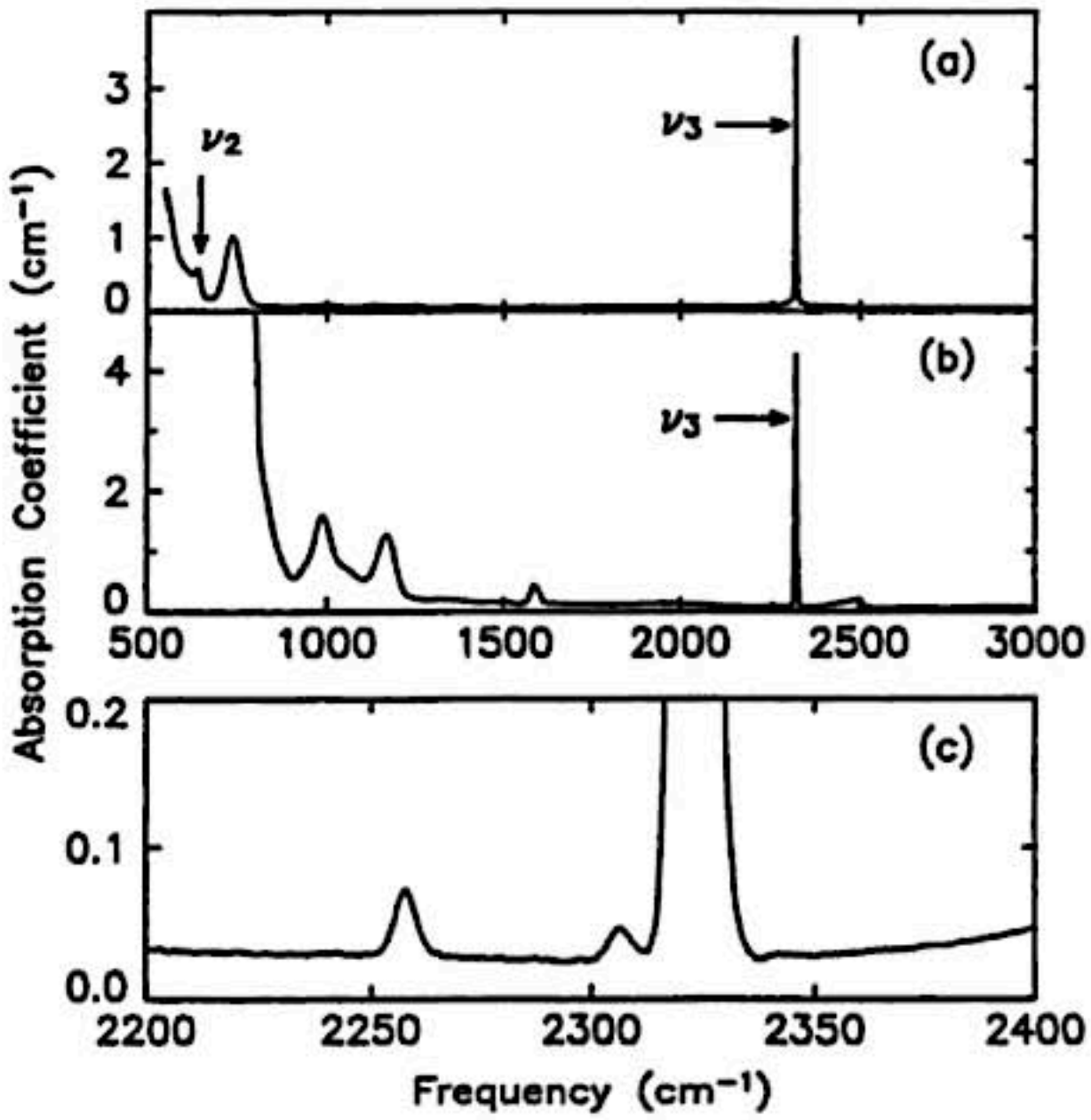

Fig. 5 Infrared absorption spectra at 1.5 K for CO_2 in (a) *a*-Se and (b) As_2S_3. The CO_2 bending mode (ν_2) and asymmetric stretch mode (ν_3) absorptions are indicated with arrows. All other absorption features are present in the undoped glass. (c) Enlarged view of the ν_3 region in As_2S_3, showing the $^{13}C^{16}O_2$ and $^{18}O^{12}C^{16}O$ isotope lines.

of 2323.2 cm^{-1}, one predicts frequencies of 2257.3 cm^{-1} and 2305.9 cm^{-1} for the asymmetric stretch in $^{13}C^{16}O_2$ and $^{18}O^{12}C^{16}O$, respectively, in excellent agreement with the observed bands. Finally, note the weak band at 641 cm^{-1} in Se shown in Fig. 5 (a). This band, not present in the undoped material, is undoubtedly the CO_2 bending mode (denoted ν_2), its position in good agreement with the gas phase value[33] of 667.379 cm^{-1}. The nature of this defect center is thus quite clear; it consists of a CO_2 molecule trapped in a cage formed by the glass matrix. The absence of any rotational structure, which dominates the gas phase spectrum, indicates that each trapped molecule is locked in fixed orientation.

The next class of defects we will examine are the hydrogen-related centers, produced by melting the glass in hydrogen gas. Figure 6 (a) shows the infrared absorption spectra at 1.5K for two samples of As_2S_3, one prepared in hydrogen, the other in deuterium. The hydrogen-doped sample displays an asymmetric absorption band peaked at 2485 cm^{-1} with a width (FWHM) of 74 cm^{-1}. The absorption band in the deuterated

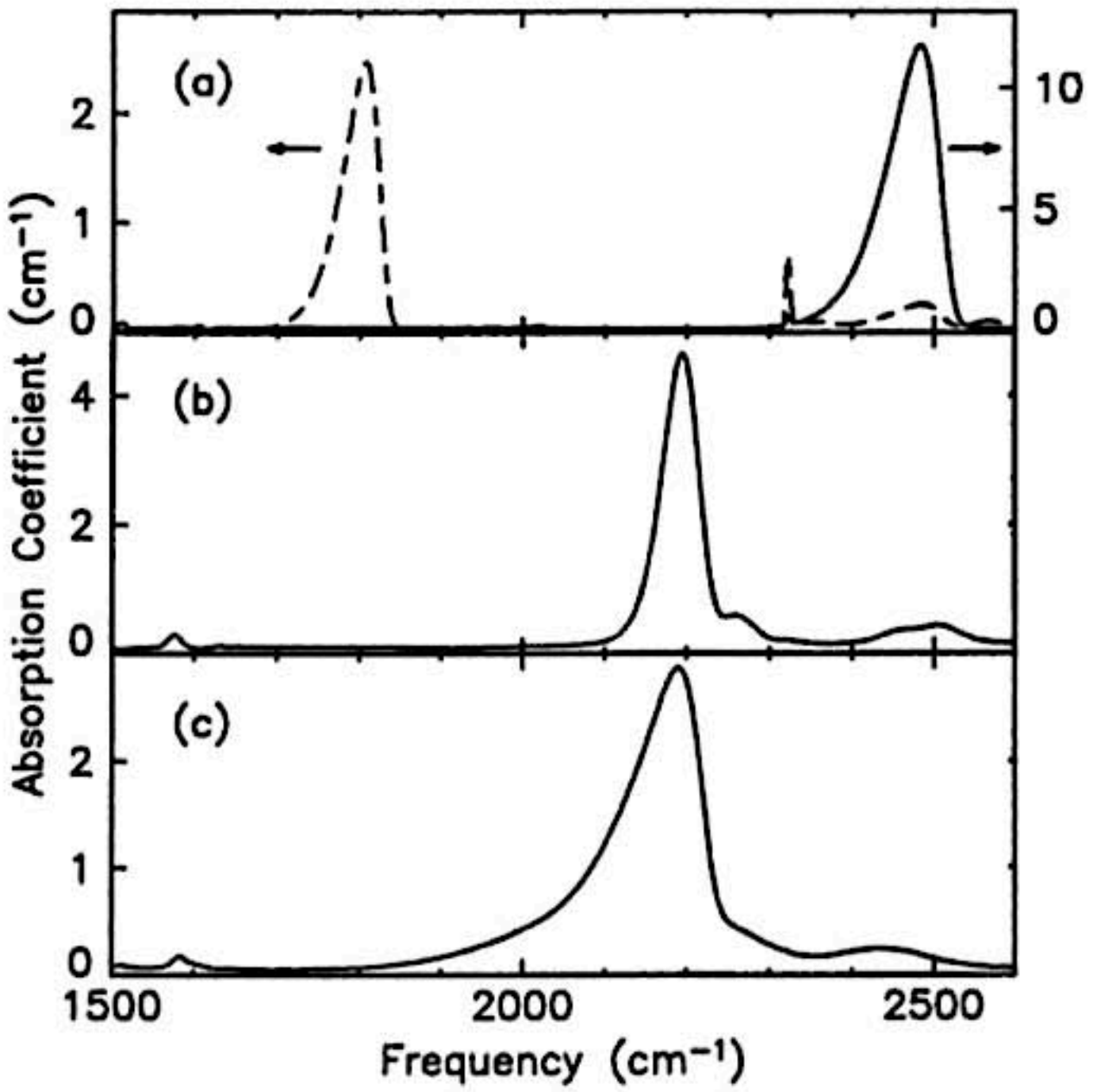

Fig. 6 Infrared absorption spectra for the hydrogen-related centers in chalcogenide glasses. (a) Absorption bands in As_2S_3 due to SH (solid line, right scale) and its deuterated analog, SD (dashed line, left scale). (b) SeH in *a*-Se. (c) SeH in As_2Se_3. Weak lines at 1580 and 2323 cm^{-1} are due to unwanted CO_2 and H_2O impurities.

sample has a similar asymmetric shape, but is peaked at 1807 cm^{-1} and has a width of 51 cm^{-1}. The isotope shift by a factor of 1.375, approximately the square root of the ratio of the masses, confirms that these absorption bands originate from vibrational transitions. These bands lie in the characteristic frequency ranges for the sulfur-hydrogen and sulfur-deuterium stretching vibrations. For comparison, gas-phase measurements[34–36] on SH and SD free radicals yield stretch mode frequencies of 2598.77 cm^{-1} and 1885.8 cm^{-1}, respectively.

In Fig. 6 (b) the result of treating Se in hydrogen is shown. Again, the doping produces a broad absorption band, this time centered at 2194 cm^{-1}, with a width (FWHM) of 53 cm^{-1}. The good agreement of the position of the band with the known SeH stretch frequency[37] implies that, as in the case of As_2S_3, the absorption band arises from hydrogen which has reacted with the host material, this time forming SeH bonds. Preparation in deuterium gas produces the expected isotope shift, the new band appearing at 1589 cm^{-1}. The origin of the weaker bands apparent in Fig. 6 (b) is not known, but they also show the isotope shift in the deuterated sample, and so they also must arise

from hydrogen vibrations.

Similar results are obtained for hydrogenated As_2Se_3, shown in Fig. 6 (c). The absorption band again appears in the SeH stretch region, this time peaked at 2189 cm^{-1}. The width of this inhomogeneous band, however, 108 cm^{-1}, is over twice that in *a*-Se, and the asymmetric shape seen for As_2S_3 is even more evident here.

The exact nature of the hydrogen-related centers is not so easily determined as was the case for CO_2. It is clear from the vibrational frequencies and isotope shifts that in each case a hydrogen atom bonded to a chalcogen atom is involved. The existence of a single strong absorption band, without any of the lower frequency bands one would expect for the bending modes of polyatomic species (such as H_2S, for instance), argues strongly that only one hydrogen atom and one chalcogen atom are involved in these centers. What cannot be determined definitively from this work is whether these centers are simple SH or SeH diatomics trapped in a matrix cage, analogous to the CO_2 centers, or whether the chalcogen involved is actually bonded to, and forms a part of, the glass matrix. The latter possibility is favored by the PIRSH burning results to be presented here, which suggest the existence of strong coupling between these defects and the glass host.

The final defects to be considered here are those produced when As_2S_3 is doped with D_2O. The choice of D_2O rather than ordinary water is one of convenience; the laser frequencies currently at our disposal do not coincide with H_2O absorption bands. Three strong absorption bands are produced by D_2O doping, as shown in Fig 7. Two of these,

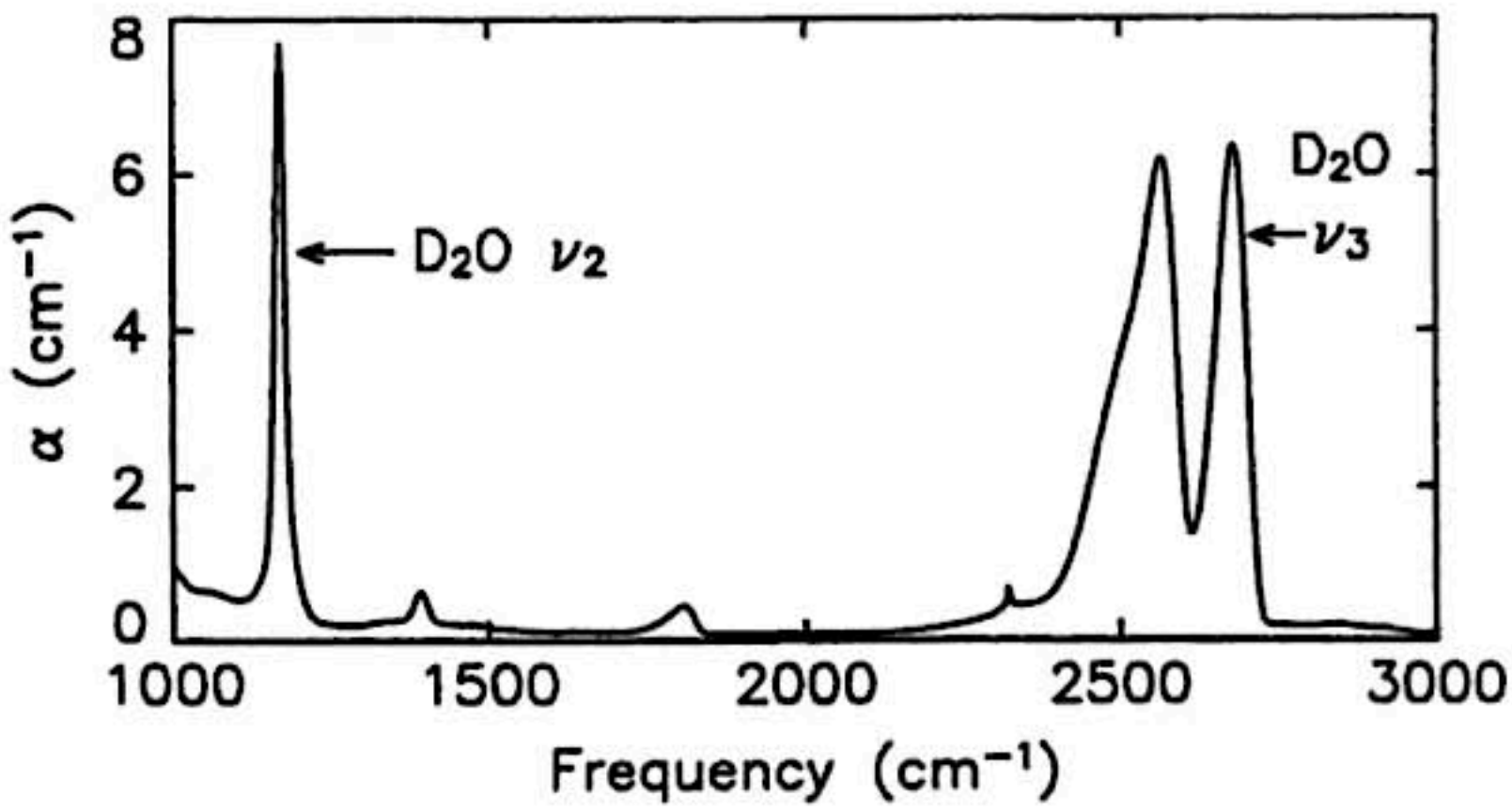

Fig. 7 Infrared absorption spectra for As_2S_3 treated in D_2O. The D_2O bending (ν_2) and stretching (ν_3) absorptions are marked with arrows. The third strong band, peaked at 2566 cm^{-1}, is tentatively attributed to OD. Weaker bands are due to unwanted impurities (see text).

centered at 1170 cm^{-1} and 2679 cm^{-1} and marked with arrows in Fig. 7, are found to maintain constant relative strengths for various sample preparations. These are assigned to the D_2O bending (ν_2) and asymmetric stretch (ν_3) modes, respectively, which have gas phase frequencies[37] of 1178 cm^{-1} and 2788 cm^{-1} . The third strong absorption band, peaked at 2566 cm^{-1}, is found to have strength which varies from sample to sample independently of the other two, being strongest in samples prepared at lower temperatures. This band is tentatively identified as arising from a simple OD stretch, but the ambiguity about the exact nature of the defect seen for the SH and SeH centers applies here also. The spectrum is complicated somewhat by unwanted impurities. These, however, are easily identified: The shoulder visible on the low frequency side of this band arises from a small amount of the SH impurity present in the starting material (compare Fig. 6 (a)). Likewise, a weak SD band is apparent at 1807 cm^{-1}, as is the sharp CO_2 absorption at 2323 cm^{-1}. The remaining small peak visible in Fig. 7, at 1393 cm^{-1}, arises from the bending mode of the mixed isotope water molecule HDO.

The inhomogeneous absorption bands shown in Fig. 5 through Fig. 7 display a wide range of lineshapes and widths, indicating a considerable variety in the way the defect is coupled to the host. Such a variety is desirable if one wishes to test the hypothesis that reconfiguration of the glass host is responsible for the hole burning. If

Table 1. IR absorption band positions, inhomogeneous widths and hole widths at 1.5 K for vibrational modes of various impurities in chalcogenide glasses.

Host	Impurity	Peak Frequency (cm^{-1})	Width (FWHM) (cm^{-1})	Hole Width (FWHM) at 1.5K (GHz)
As_2S_3	$^{12}C^{16}O_2$	2323.2	6	0.080 ± 0.003
	$^{13}C^{16}O_2$	2258.0	6	—
	$^{18}O^{12}C^{16}O$	2306.5	6	—
a-Se	$^{12}C^{16}O_2$	2321.0	6	0.080 ± 0.005
		641	~ 20	—
As_2S_3	SH	2485	74	0.8 – 15 *
	SD	1807	51	0.6 *
a-Se	SeH	2194	53	0.81 – 8.5 *
	SeD	1589	33	—
As_2Se_3	SeH	2189	108	1.1 – 10 *
As_2S_3	D_2O	2679	59	1
		1170	19	—
	OD	2566	95	1

*Depends on burn frequency. Range indicated is merely that observed to date; actual upper limit is probably much greater. See text.

this model is valid, one expects that hole burning behavior, in particular the distribution of barriers between the burned and unburned configurations, should be similar for all defects in a given host.

Persistent Spectral Hole Burning Results

In this section we will first summarize the rudimentary PIRSH burning behavior at low temperatures for the various systems. We will then compare the temperature dependences and relaxation behaviors for those systems where direct comparison is appropriate.

CO_2 in As_2S_3 and a-Se.

Figure 8 shows the PIRSH produced in the asymmetric bending mode absorption of CO_2 in As_2S_3 by burning at three different temperatures, 1.6 K, 21 K and 46 K. The laser frequency, 2324.2 cm^{-1}, lies 1 cm^{-1} to the high frequency side of the peak of the inhomogeneous band. Plotted is the change in the absorption coefficient α produced by

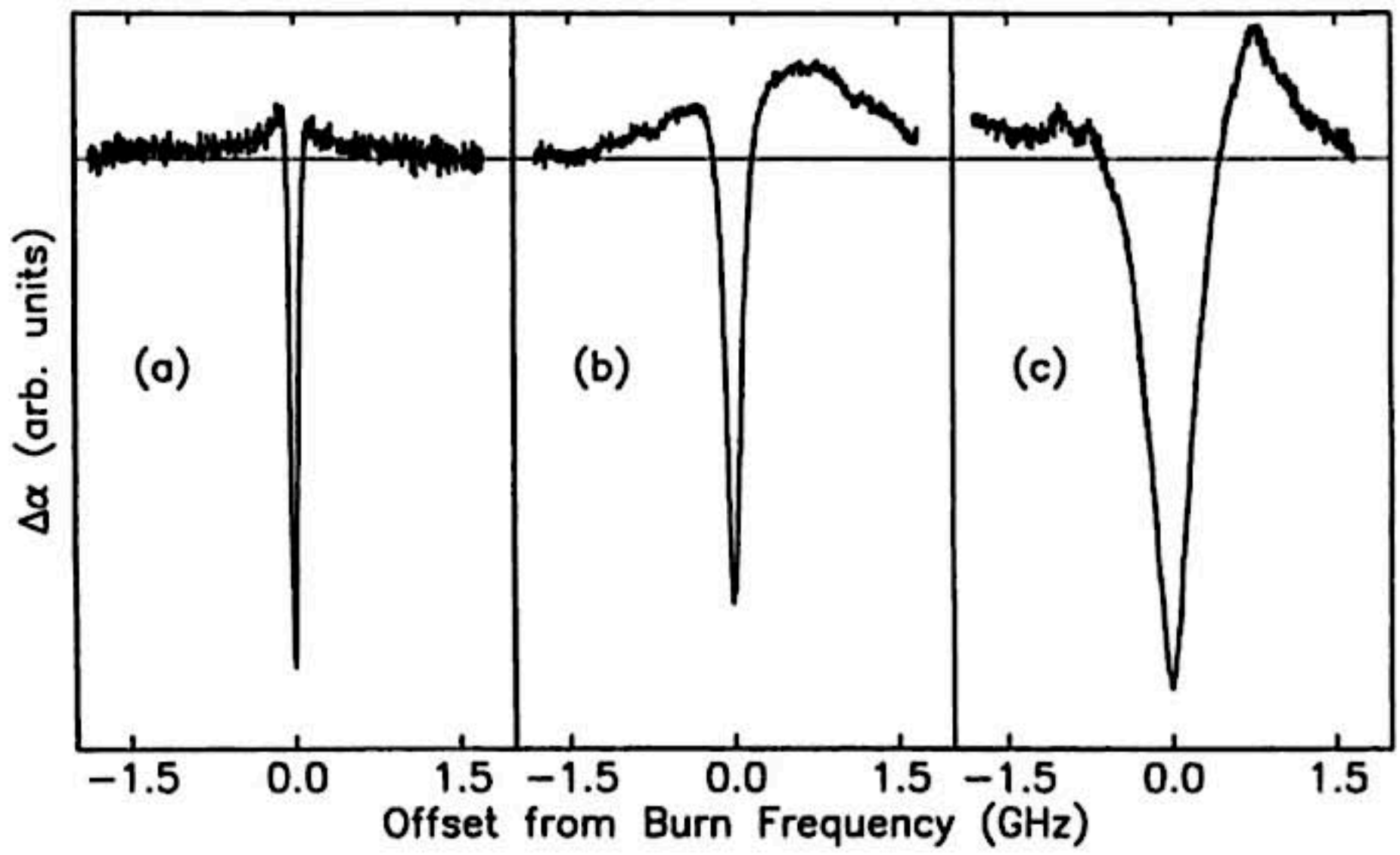

Fig. 8 PIRSH burning in the ν_3 mode of CO_2 in As_2S_3 at temperatures of (a) 1.6 K, (b) 21 K, and (c) 46 K. Plotted is the laser-induced change in absorption coefficient as a function of the offset from the burn frequency. The horizontal straight line indicates zero absorption change. Note holes (absorption decrease) and antiholes (absorption increase) in each case. Vertical scales have been adjusted to facilitate comparison; actual hole depths are 0.047, 0.016, and 0.003 cm^{-1}, respectively.

the laser irradiation, as a function of the offset from the burn frequency. Burning and probing of the hole are performed at the same temperature in all cases. The horizontal line in Fig. 8, shown for reference, represents zero change in absorption. Note that in addition to the hole (negative $\Delta\alpha$) centered at the burn frequency there is in each case a much broader antihole (positive $\Delta\alpha$) indicating the new frequency location for those centers which have been hole-burned. The observation of antiholes so near in frequency to the original hole shows that the hole burning process is not photochemical in nature. The location of the antihole appears to shift to higher frequency with increasing temperature, a behavior not yet understood.

The width of the hole at 1.6 K is 80 ± 3 MHz, the narrowest hole observed to date in the chalcogenides. This width does not appear to depend on the burn frequency used. The width increases to 166 ± 5 MHz at 21 K and to 520 MHz at 46 K. Above this temperature, observation of the holes becomes difficult as they become increasingly broader, shallower and shorter lived. Heating above 60 K for a few minutes effectively erases holes burned at any temperature in this system.

Preliminary studies of the same defect in *a*-Se show that the 1.6 K hole width for CO_2 in *a*-Se is virtually identical to that in As_2S_3.

Hydrogen-related Centers in As_2S_3, As_2Se_3 and a-Se.

As seen by linear spectroscopy, the most obvious difference between the hydrogen-related centers and the CO_2 centers, regardless of host, is the enormous difference in the inhomogeneous linewidths, those for the SH and SeH centers being an order of magnitude greater than than those for CO_2. PIRSH burning experiments reveal a similar order of magnitude difference in the homogeneous widths. In addition, however, the hole widths for SH and SeH show a strong dependence on the burn frequency. This behavior is shown in Fig. 9(a) for the SH center in As_2S_3, and in Fig. 9(b) for the SeH center in both As_2Se_3 and *a*-Se. For SH in As_2S_3 at 1.5 K, the hole width in the low intensity, short burn time limit shows a minimum of 0.8 GHz for burns at 2525 cm^{-1}, near the high-frequency limit of the inhomogeneous band. The width increases sharply with decreasing laser frequency, reaching 8 GHz at 2445 cm^{-1}, and eventually exceeding the diode laser's continuous tuning range of roughly 15 GHz.

As can be seen in Fig. 9(b), the frequency dependence of the hole width for SeH centers in the Se and As_2Se_3 glasses is remarkably similar to that of the SH center. The hole width at 1.5 K for SeH in *a*-Se is 0.81 ± .05 GHz for burns at 2221 cm^{-1}, while at the same frequency the width for the SeH center in As_2Se_3 is 1.08 ± .05 GHz. As with the SH centers, the width for the SeH centers in both hosts increases sharply with decreasing burn frequency. The ratio of the hole width in As_2Se_3 to that in *a*-Se maintains a value of roughly 1.4 which is nearly constant, within experimental error, for

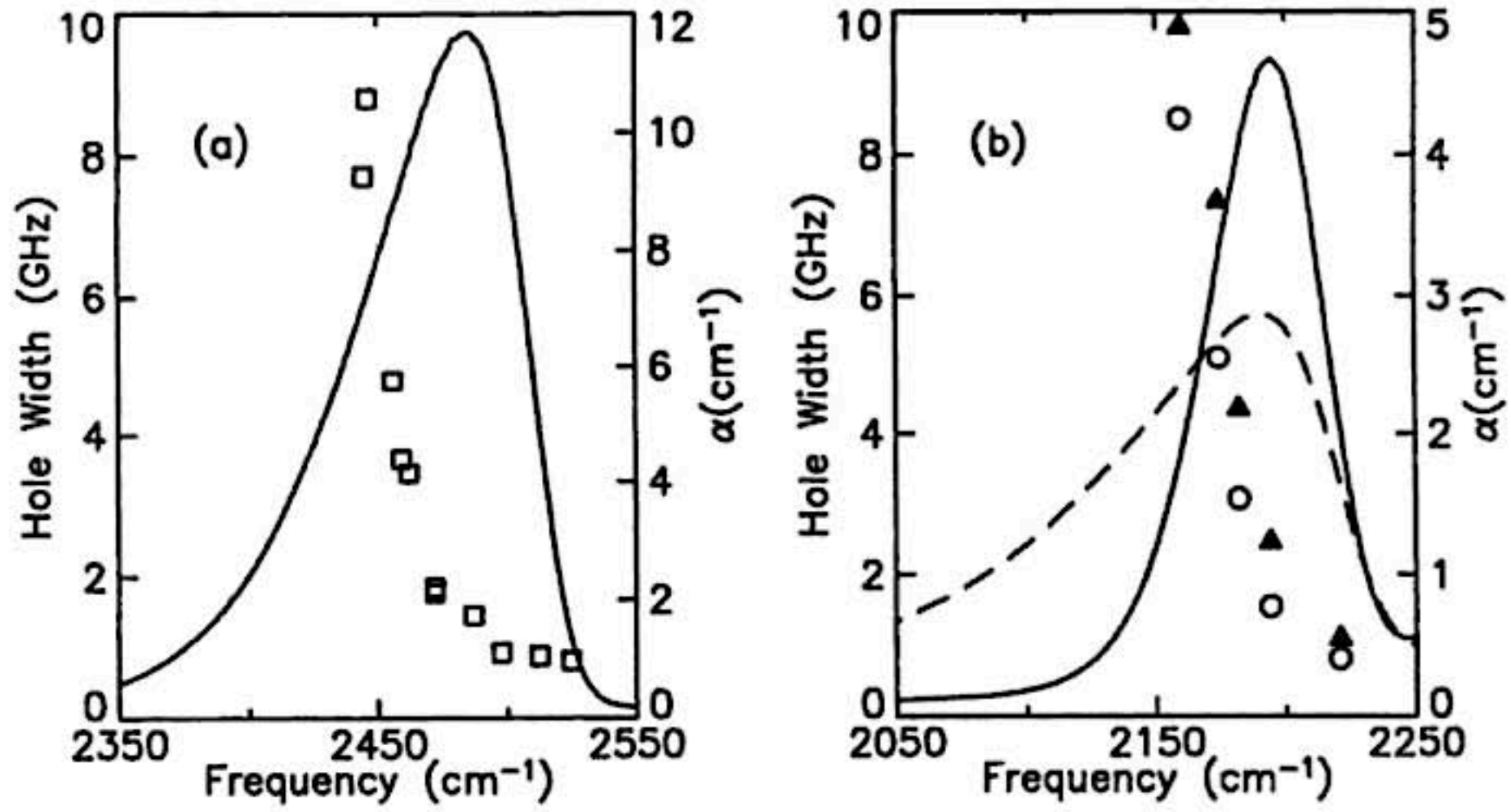

Fig. 9 Hole width at 1.5 K as a function of burn frequency for hydrogen-related centers in As_2S_3, As_2Se_3, and *a*-Se. (a) Hole width (squares, refer to scale on left) and absorption spectrum (solid line, refer to scale on right) for SH in As_2S_3. (b) Hole widths and absorption spectra for SeH in As_2Se_3 (triangles, dashed line) and in *a*-Se (circles, solid line). Hole widths are in the small hole limit.

all burn frequencies.

As was the case for CO_2 in As_2S_3, holes burned in the SH mode in As_2S_3 and the SeH mode in As_2Se_3 can be erased by heating the sample to roughly 60 K for approximately a minute. The SeH mode in *a*-Se, however, shows markedly different thermal erasure behavior; complete erasure of holes in this material is obtained only after heating to about 80 K.

A novel phenomenon so far observed only for the SH center in As_2S_3 is the narrowing of the hole with time after the burning laser is removed. The effect is shown in Fig. 10. It should be noted that, unlike the results discussed above, the holes in this case are not produced in the short time low intensity limit; the hole narrowing phenomenon is seen only for relatively long burns (several minutes) at high intensities. This behavior is the opposite of the more typical hole broadening which has been observed in several electronic hole burning systems and attributed to spectral diffusion.[30] It thus seems unlikely that significant slow spectral diffusion processes are occurring after the hole has been burned. This eliminates one possible effect which might prevent true homogeneous widths from being determined from the hole widths. It is still possible, of course, that spectral diffusion on short time scales could occur during the burning process.

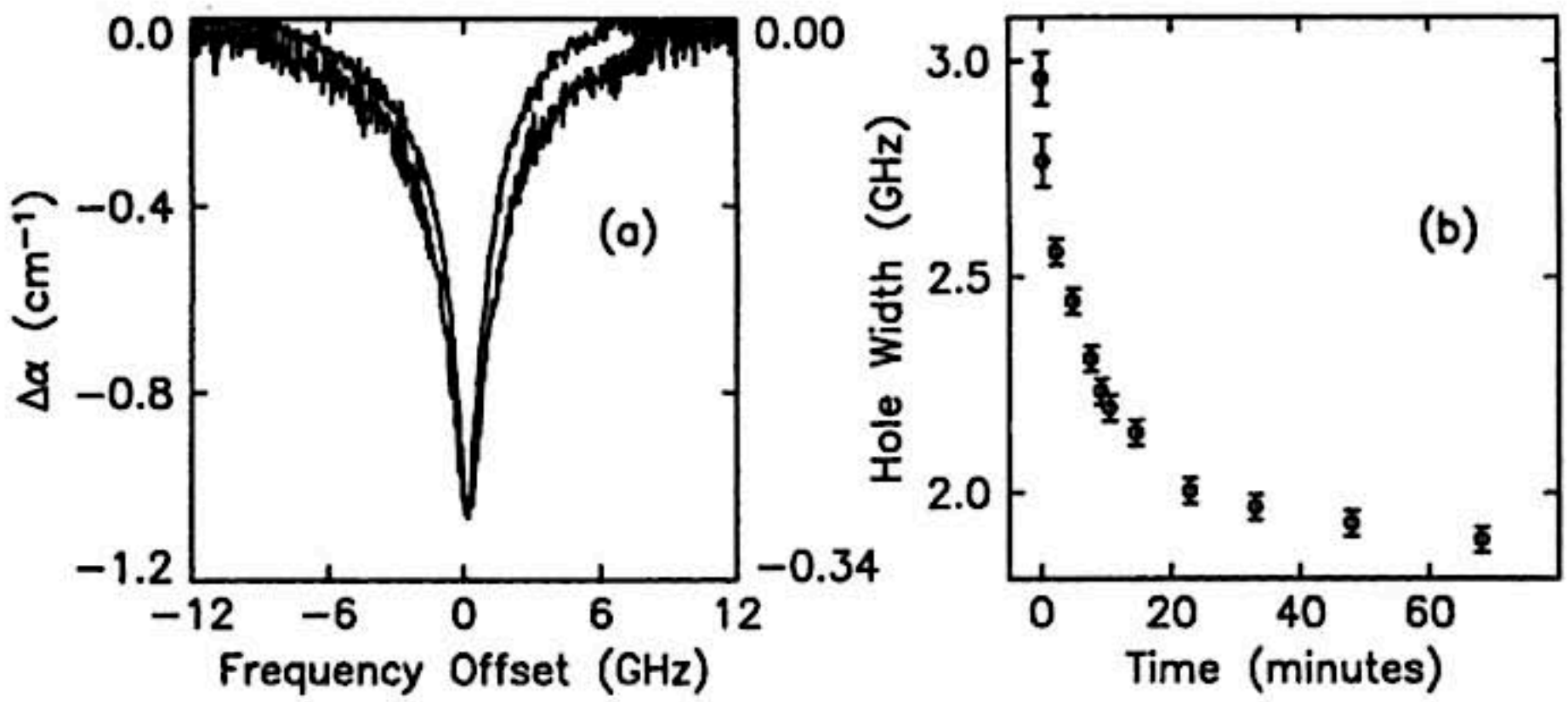

Fig. 10 Time evolution of the hole width in the deep hole regime for SH in As_2S_3. (a) The appearance of the hole 5 seconds (broad hole) and 48 minutes (narrow hole) after the burning laser is removed for a hole burned 5 minutes at 2504 cm^{-1}. The vertical scale for the narrow hole has been expanded by a factor of 3.5 to facilitate comparison. Reduced noise in the 48 minute hole is the result of long signal averaging times not possible with the rapidly changing short time hole. (b) Hole width as a function of time after burning ceases.

One possible explanation for the hole narrowing behavior is that centers absorbing at a given frequency have a distribution of homogeneous widths, with those centers having greater homogeneous widths (i.e. faster dephasing) relaxing more rapidly from the burned to the unburned configuration. This possibility emphasizes the fact that hole burning merely selects out centers with identical absorption frequencies, and does not necessarily, as is sometimes mistakenly believed, select centers with identical environments.

D_2O and OD in As_2S_3.

PIRSH burning has been observed for the 2679 cm^{-1} D_2O stretch band with hole widths at 1.5 K on the order of 1 GHz. The 2566 cm^{-1} OD stretch band also exhibits PIRSH burning, with similar hole widths. As is the case with other defects in As_2S_3, these holes are completely erased by heating to 60 K. Although at the time of this writing these two defects have not been as extensively studied as the others, the fact that they too exhibit PIRSH burning provides important confirmation of the generality of this phenomenon in chalcogenide glasses.

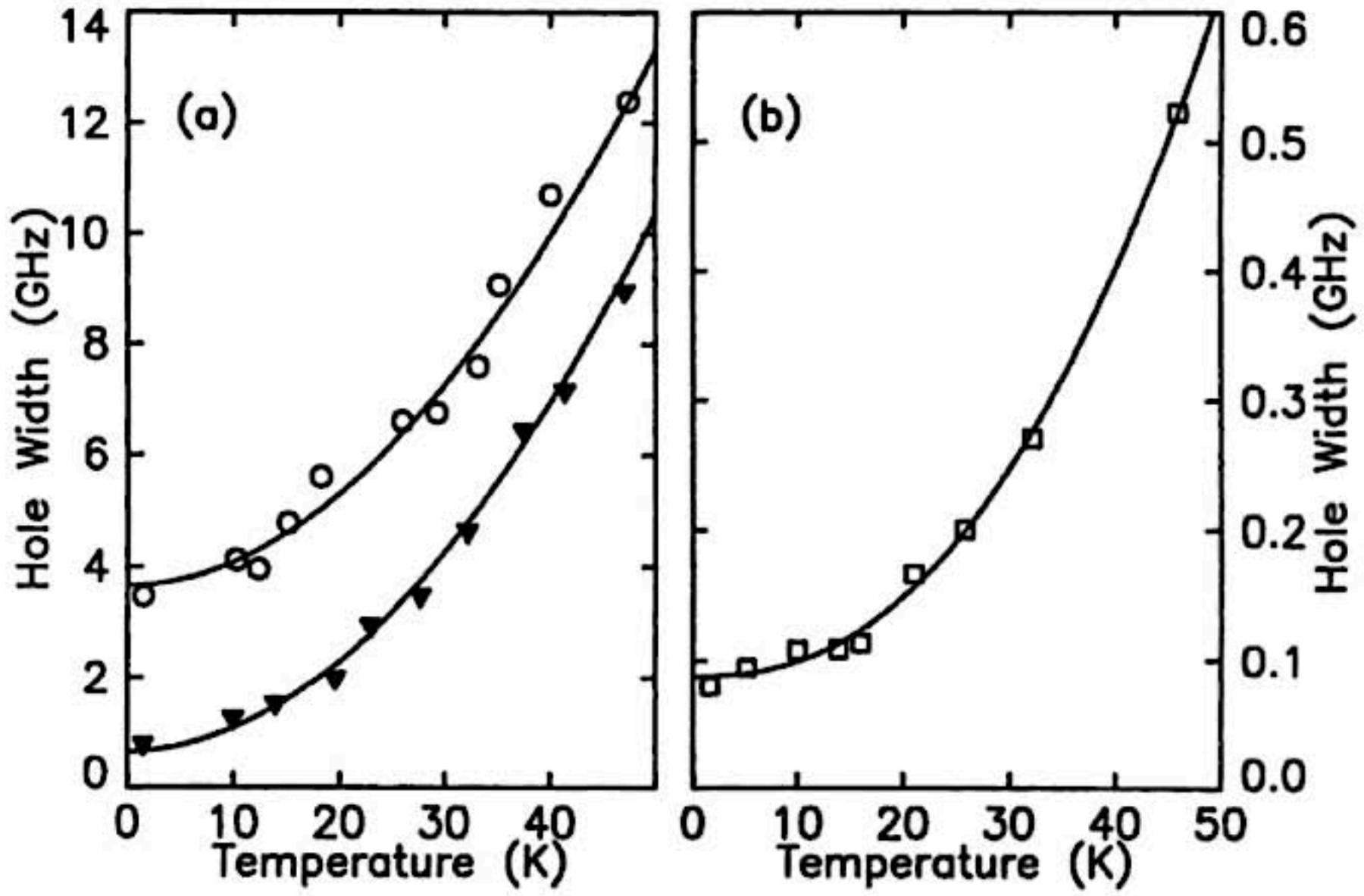

Fig. 11. Temperature dependence of the hole width in As_2S_3. (a) SH in As_2S_3 at two different burn frequencies: 2504 cm^{-1} (triangles) and 2462 cm^{-1} (circles). (b) CO_2 in As_2S_3. Burn frequency is 2324 cm^{-1}. Hole widths are in the small hole limit. Solid lines are power law fits described in the text.

Temperature Dependence of the Hole Width.

Despite the considerable differences in the homogeneous and inhomogeneous widths for CO_2 and SH in As_2S_3, and the strong burn frequency dependence of the hole width observed for the latter, the temperature dependences of the hole width of these two defects in this host are remarkably similar. Figure 11(a) shows the hole width as a function of temperature for the SH defect in As_2S_3 for two burn frequencies. The temperature dependence of the hole width for CO_2 in As_2S_3 is shown in Fig. 11(b). In all cases the hole is burned and probed at the same temperature.

In each case note that the hole width does not appear to vanish as T approaches zero, but rather approaches a finite value not significantly smaller than the width at 1.5 K. Above this low temperature value, which is presumably determined by the excited state lifetime, the hole width increases approximately as T^2. The hole width $\Delta\nu$ (T) is well described, over the entire temperature range studied, by a power law of the form

$$\Delta\nu\,(T) = \Delta\nu_0 + a\,T^b\,. \qquad (12)$$

The best fit for CO_2 in As_2S_3 is obtained with $\Delta\nu_0 = 80$ MHz, the temperature exponent

b =(2.2 ± 0.3), and a = 0.096 MHz / $K^{2.2}$, as shown by the solid line in Fig. 11(b). Fits to the two data sets for the SH defect in As_2S_3 yield the following values: temperature exponent b = (1.97 ± .1), and the coefficient a = 3.4 x 10^{-3} GHz/ $K^{1.97}$. The zero temperature widths are $\Delta\nu_0$ = 0.8 GHz and $\Delta\nu_0$ = 3.6 GHz for the 2503 cm^{-1} and 2462 cm^{-1} data, respectively. Note that for the two burn frequencies shown for the SH defect, only $\Delta\nu_0$ differs, while a and b are apparently independent of the burn frequency.

Though the temperature dependences for two different defects in As_2S_3 are virtually identical, the behavior in a different host, *a*-Se, shows obvious differences. Figure 12 shows the hole width as a function of temperature for the SeH defect in *a*-Se between 1.6 K and 56 K for holes burned at 2209 cm^{-1}. For comparison, the 2503 cm^{-1} data for SH in As_2S_3 are also included. Figure 12(a) shows these data plotted with linear axes. The *a*-Se:SeH data can again be fit over the entire temperature range using Eq. 12, but the hole width no longer goes as T^2. Instead the fit yields temperature exponent b = (1.27 ± 0.1), with $\Delta\nu_0$ = 0.79 GHz, and a = 0.11 GHz/ $K^{1.27}$. The difference in the power law behavior for the two hosts is emphasized in Fig. 12(b), which plots the same data on log-log axes with $\Delta\nu_0$ first subtracted off. It is clear that, although the hole width

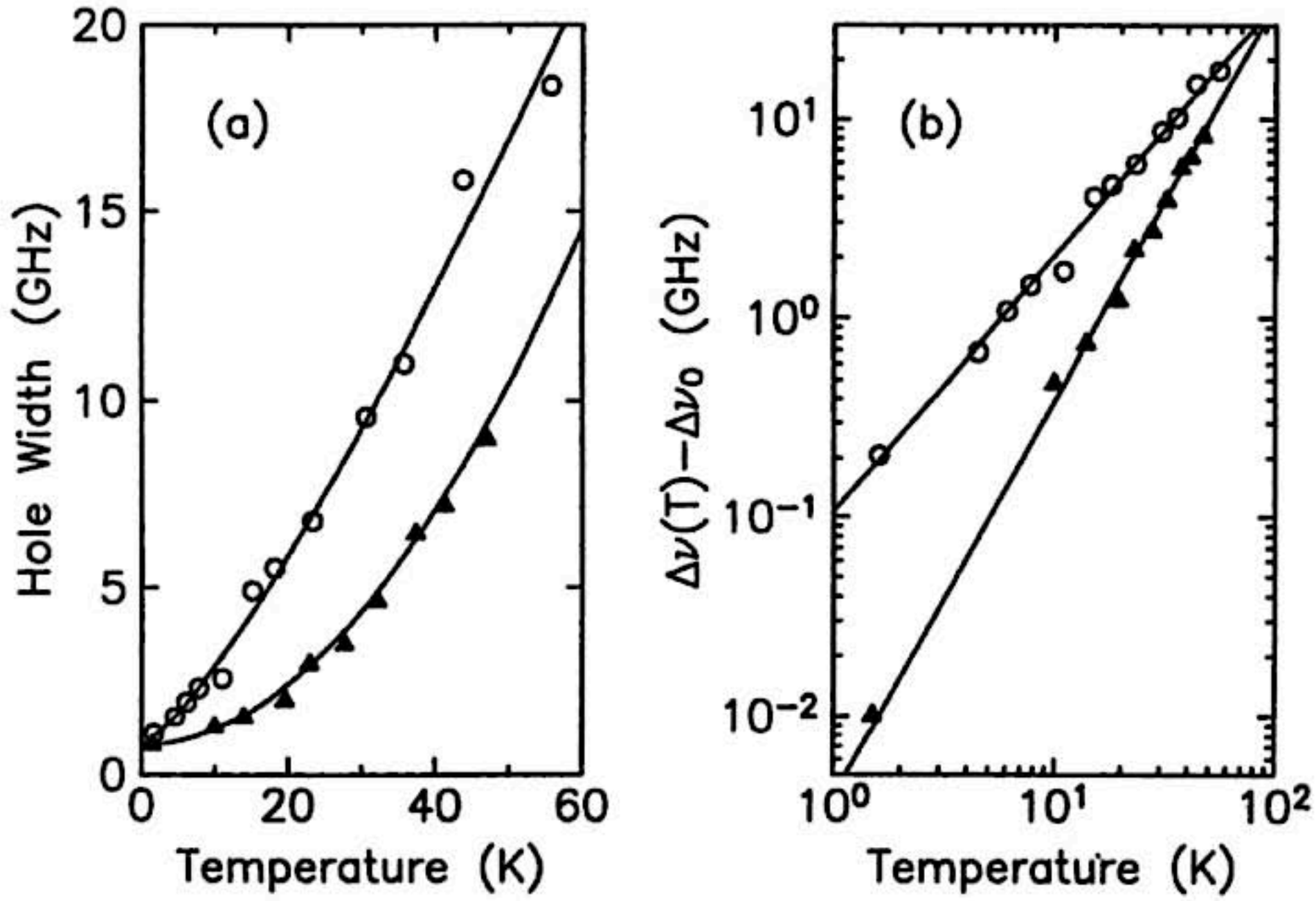

Fig. 12. Comparison of the temperature dependence of the hole width for SeH in *a*-Se (circles) and SH in As_2S_3 (triangles). (a) Total hole width, plotted on a linear scale. (b) The same data plotted on logarithmic axes, after first subtracting the zero temperature hole width. Solid lines are power law fits described in the text.

for *a*–Se:SeH increases more rapidly with temperature than does that for As_2S_3:SH, it does so in a more nearly linear fashion.

Spontaneous Hole Filling.

After burning ceases, PIRSHs burned in all these systems are observed to decay in a strongly non-exponential manner. One aspect of the PIRSH burning behavior of molecular impurities in chalcogenide glasses which sets these systems apart is that the spontaneous relaxation from the burned to unburned configurations takes place on an experimentally accessible time scale, allowing this relaxation to be observed over a much wider dynamic range than in the much more slowly relaxing amorphous systems studied by other workers.

Because the inhomogeneous bands for SeH in *a*-Se and As_2Se_3 overlap in frequency (see Fig. 6) , and the defect in each case appears to be essentially the same, these two systems were chosen to determine how different hosts affect the hole relaxation behavior. The frequency overlap allows the same laser mode and identical optical setup to be used for both systems, thus eliminating artifacts introduced by differing burning intensities. Figure 13 shows the spontaneous hole decay observed at 1.5 K for the SeH defect in *a*-Se and As_2Se_3 after identical 3 minute burns at 2194 cm^{-1} with an intensity of roughly 250mW/cm^2. Plotted here is the integrated hole area, proportional to the number of centers remaining in the burned configuration, as a function of time after burning ceases. The hole area is normalized to unity at t = 0.

The data shows that, though the two systems appear nearly identical in other respects, the host plays a decisive role in determining the relaxation rates between the ground state configurations. Though both systems display strongly non-exponential hole decay, the relaxation in *a*-Se is more nearly exponential and is dominated by rates three orders of magnitude slower than that in As_2Se_3.

In order to clarify the meaning of the spontaneous hole filling data, it is instructive to apply the following simple model. Because the hole decay is observed to be independent of temperature below 10 K, it is reasonable to assume that the decay proceeds by tunneling between the ground state configurations. The rate at which a given center relaxes from the burned to the unburned configuration is given by

$$\Gamma_{BU} = \Gamma_0 e^{-\lambda} \tag{13}$$

where Γ_0 is an attempt frequency, assumed to be on the order of a phonon frequency, and λ is the tunneling parameter, of the general form $(2mV)^{1/2}d/\hbar$ where m is the mass of the tunneling entity, V the barrier height, and d the width of the barrier. In order to take into account the distribution of environments seen by the defect, we shall simply

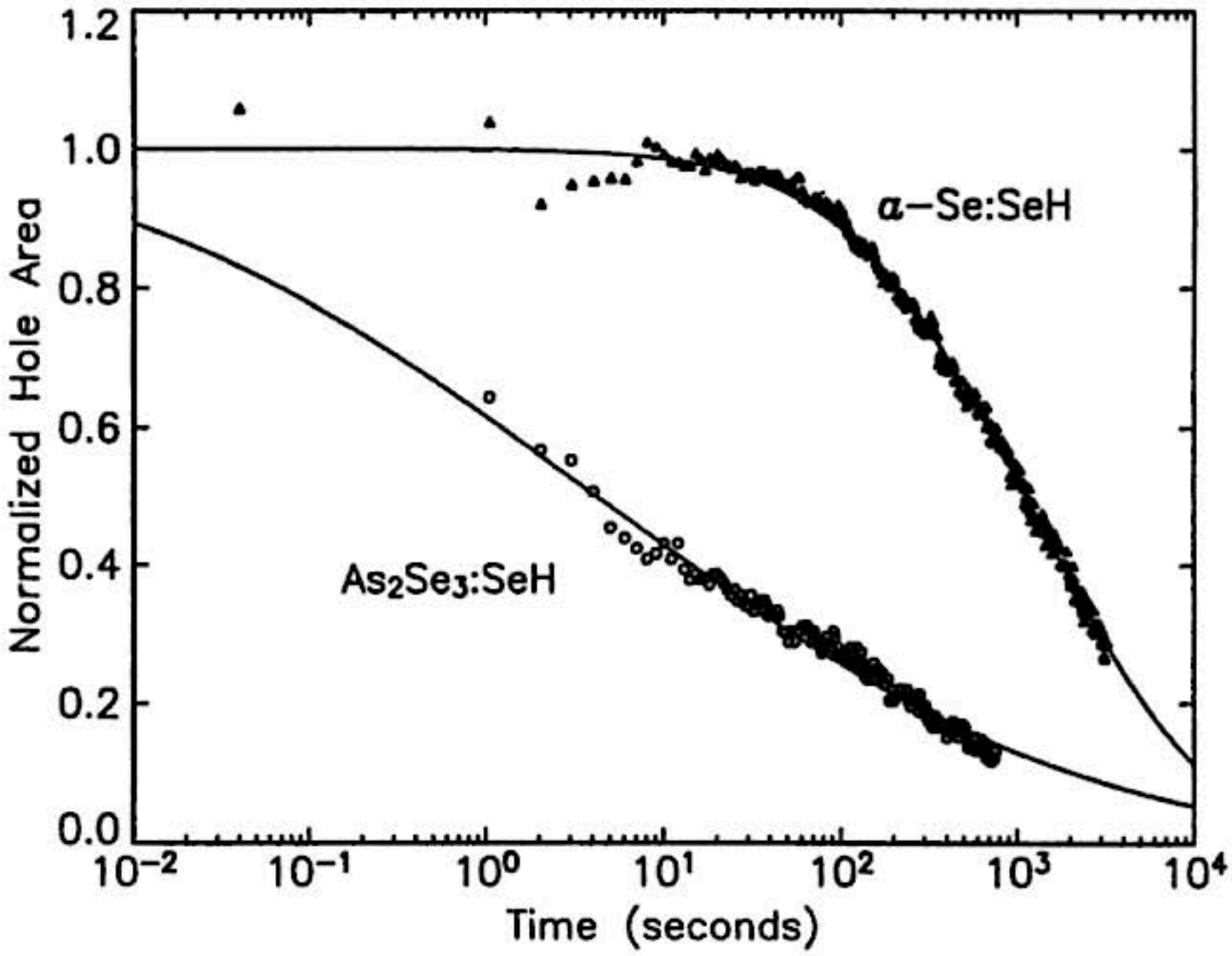

Fig. 13. Spontaneous hole decay at 1.5 K for the SeH defect in *a*-Se (triangles) and in As_2Se_3 (circles). Holes in the two systems were burned at 2194 cm^{-1} under identical conditions. Solid lines are fits to Eq. 16 (see text). Hole area is normalized so that fits extrapolate to unity at t = 0.

allow, as suggested by Jankowiak, et al.,[38,39] the tunneling parameter λ to assume a Gaussian distribution about some center value λ_0:

$$G(\lambda) = (1/\pi^{1/2}\sigma) \exp [- (\lambda - \lambda_0)^2 / \sigma^2] . \qquad (14)$$

Thus if $N_B(0)$ is the total number of centers initially in the hole-burned state, the number of centers having burned-to-unburned relaxation rates between $\Gamma_0 e^{-\lambda}$ and $\Gamma_0 e^{-(\lambda + d\lambda)}$ is $N_B(0)\, G(\lambda)\, d\lambda$. The number of centers with this relaxation rate remaining after time t is then given by

$$dN_{B,\lambda}(t) = N_B(0)\, G(\lambda)\, d\lambda \exp[- \Gamma_0 t\, e^{-\lambda}] \qquad (15)$$

and so the total number of centers remaining in the hole-burned configuration after time t is obtained by integrating Eq. 15 over all λ:

$$\frac{N_B(t)}{N_B(0)} = \frac{1}{\pi^{1/2}\sigma}\int_0^\infty \exp[-(\lambda-\lambda_0)^2/\sigma^2]\exp[-\Gamma_0 t\, e^{-\lambda}]\, d\lambda \quad . \tag{16}$$

Excellent fits to the data are obtained using Eq. 16, as is shown by the solid lines in Fig. 13. Figure 14 shows the Gaussian distributions of tunneling parameters obtained from fitting Eq. 16 to the *a*-Se:SeH and As_2Se_3:SeH decays shown in Fig. 13, with the attempt frequency assigned the value $\Gamma_0 = 10^{13}$ sec^{-1}, which is on the order of the Debye frequency for both of these systems. One may also simply view Fig. 14 as distributions of relaxation times for the two systems, as indicated by the upper axis, and simply ignore the physical assumptions contained in this model. The dashed vertical line in Fig. 14 delineates the experimentally accessible region; relaxation times to the left of this line would be too fast to be observed in this experiment. Thus, the fast relaxation side of the distribution for As_2Se_3:SeH is not well determined, and may not fall off at the faster rates as shown. The lack of any *a*-Se:SeH centers relaxing with times between 0.1 and 50 seconds, on the other hand, is unambiguously a real effect; any relaxation occurring on this timescale would have been easily observed. Figure 14 illustrates clearly that hole erasure As_2Se_3:SeH is characterized by a very broad distribution of relaxation times,

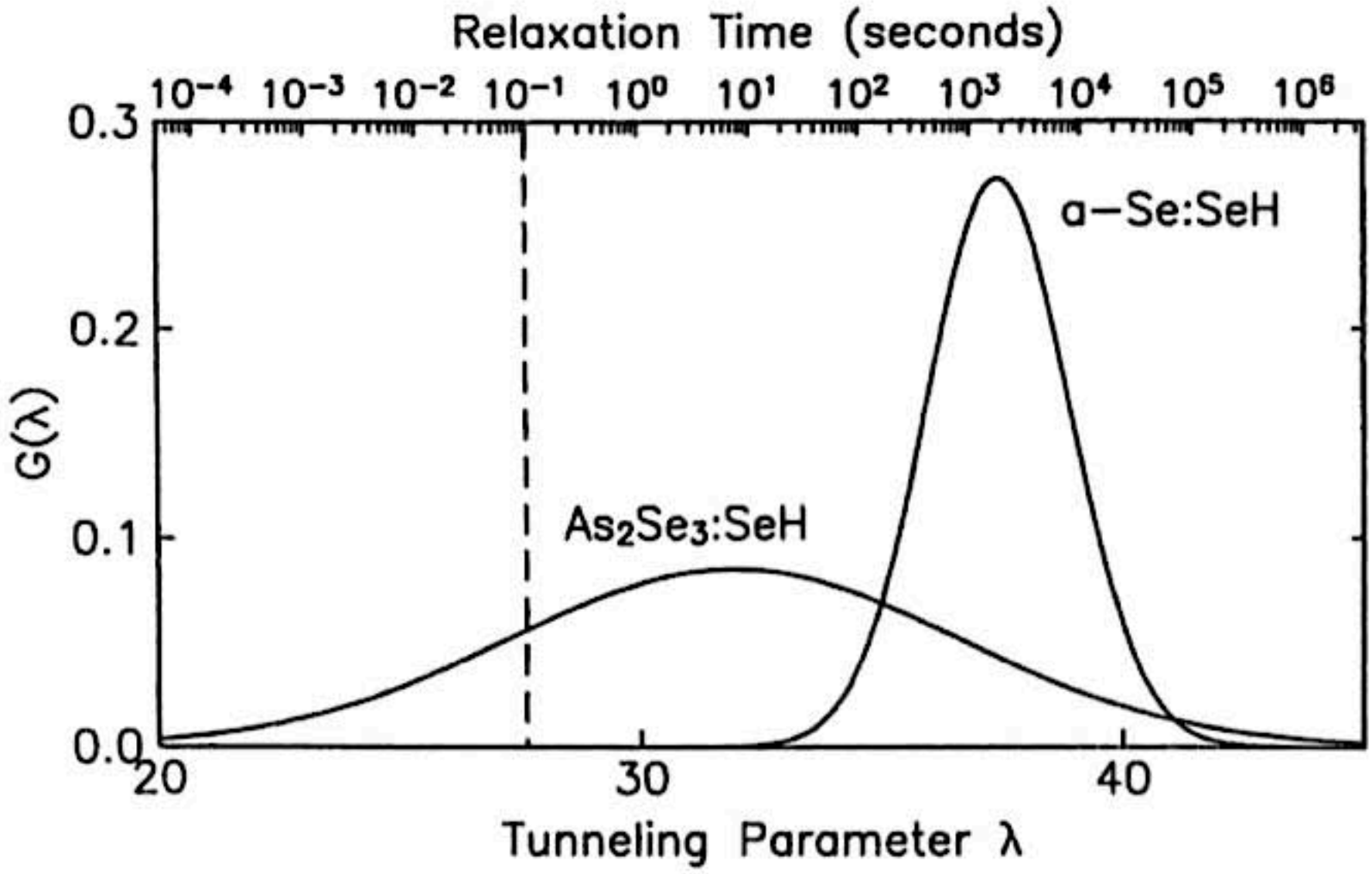

Fig. 14. Gaussian distributions of tunneling parameters extracted from fits of Eq. 16 to the data of Fig. 13, assuming an attempt frequency of 10^{13} sec^{-1} (see text). These may also be viewed as distributions of relaxation times, as indicated by the top scale. The experimentally accessible relaxation times lie to the right of the dashed vertical line.

ranging from less than 1 second to several hours, with the peak of the distribution occurring at roughly 10 seconds, while that for *a*-Se:SeH characterized by a much narrower distribution of relaxation times, peaked at roughly 2000 seconds.

Spontaneous hole refilling has also been studied for CO_2, SH, and OD in As_2S_3. Direct comparisons of relaxation behavior for different defects absorbing at different frequencies are made difficult by the fact that the laser characteristics affect the observed decay behavior to some extent. The problem can be understood by examining Eq. 6, which predicts the hole will eventually reach a steady-state depth due to the action of the third term. It should be clear that, for a given burned-to-unburned relaxation rate Γ_{BU}, there exists a minimum intensity below which the hole will be undetectably small at the steady state condition. For a system having a distribution of values for Γ_{BU}, hole burning at a particular intensity selects out only those centers which relax slowly enough to make a detectable contribution to the hole. Thus holes burned at high intensity appear to relax more rapidly than those burned at lower intensity. It is therefore important, if quantiative comparisons of hole relaxation behavior are to be made, that holes be burned with identical intensities for each system. The wide variation in the spatial power distributions of Pb-salt diode laser modes, which typically have highly non-Gaussian beam profiles, makes this quite difficult to achieve in practice. Even with this problem in mind, however, it is still possible to make the qualitative statement that the hole decay behavior for all defects in As_2S_3 is more similar to the As_2Se_3:SeH results than to those for *a*–Se:SeH. Dominant relaxation times in As_2S_3 at 1.5 K are on the order of 10 to 100 seconds and under no circumstances, even for the lowest intensity, have the slow rates and narrow distributions seen for *a*-Se been approached.

V. DISCUSSION

When taken together, these results form a pattern which lends credence to the idea that hole burning in these systems arises from restructuring of the glassy host. A diverse set of impurities in a single host all display very similar hole relaxation behavior, while identical impurities in different hosts show strikingly different behavior. Though more work is still needed to determine whether this pattern holds quantitatively for all cases, these results demonstrate the dominant role of the host in determining the hole relaxation behavior. This is in contrast to the behavior of crystalline systems which show hole burning through defect reorientation;[7,15,16] as would be expected with this mechanism, barriers to reorientation, and hence hole relaxation rates, vary widely from defect to defect in these crystalline systems, depending on the details of the molecules' size, shape, and coupling to the host. Thermal hole erasure behavior is also similar for all defects in As_2S_3, holes being erased by heating to about 60 K for a few minutes, while temperatures of roughly 80 K are required to erase holes in *a*-Se. Again this indicates

that the barriers between the burned and unburned configurations are intrinsic to the host, regardless of the defect involved.

A similar pattern emerges for the hole widths in the various systems. Although it is clear from the large difference in hole widths for the CO_2 and SH defects in As_2S_3 that the nature of the defect and how strongly it is coupled to the host determine the absolute magnitude of the hole width, the temperature dependence of the hole width appears to be determined solely by the host, independent of the defect involved, indicating that the dephasing processes responsible are intrinsic to the host.

The remarkably strong burn frequency dependence of the 1.5 K hole widths observed for the SH and SeH centers is particularly intriguing because it appears to indicate a correlation between the inhomogeneous broadening perturbation and the excited state lifetimes. In each case the inhomogeneous absorption band for the defect in the glass has an asymmetric shape with a relatively sharp high frequency cutoff at frequencies roughly 2 percent lower than the gas phase values for these molecules. This suggests an inhomogeneous broadening perturbation which acts only to reduce the vibrational frequency of the impurity molecule; i.e. the stiffness of the chalcogen-hydrogen bond may be decreased through the interaction with the host, but never increased. A comparison of the spectra for SeH in *a*-Se and in As_2Se_3 supports this idea, since the increased broadening in As_2Se_3 extends only the low frequency side of the inhomogeneous band. Thus, in this picture, relatively unperturbed molecules weakly coupled to the host are responsible for absorption on the high frequency side of the inhomogeneous band, while absorption in the low frequency tail arises from strongly coupled, highly perturbed molecules. The increase in hole width with decreasing burn frequency is a reflection of the increased host-defect coupling strength at the lower frequencies. This appears reasonable, since one would expect both the defect's excited state lifetime T_1 and the pure dephasing time T_2^* to depend to some extent on the coupling strength, with stronger coupling allowing faster dephasing as well as faster decay of the defect vibration through energy transfer to the host. T_1 should be essentially independent of temperature, while T_2^* should be stongly temperature dependent since dephasing processes involve thermally populated excitations in the host. The fact that the temperature dependent contribution to the hole width is observed to be of the same form and magnitude for both the broad low frequency holes and for the narrow high frequency holes in the As_2S_3:SH system (Fig. 11) suggests that it is mainly the excited state lifetime which is responsible for the strong frequency dependence of the hole width. If this is correct, the interesting puzzle is what decay mechanism can be responsible for such short vibrational lifetimes. The most obvious mechanism, multiphonon decay, is apparently ruled out by the fact that the smallest hole width observed for the SD defect in As_2S_3 is 0.6 GHz, compared to 0.8 GHz for SH; since multiphonon decay would be an eight-phonon process for SH and a more strongly allowed five-phonon process for SD, this

mechanism should lead to a broader hole in the deuterated case, not a narrower hole as observed.

Future Prospects

From the results obtained so far, it appears that the chalcogenides hold promise for unraveling some of the general problems of persistent hole burning in glasses. Much work has been done over the past decade on PSHB of electronic transitions in a wide variety of amorphous systems, and, though some more or less universal features of the PSHB behavior have been uncovered, other aspects show wide variability from system to system. Relating the hole burning behavior to other physical properties of the various glasses has remained an elusive goal, in part because the systems in which PSHB has been observed are so diverse, relatively unrelated, and not yet numerous enough, and have presented little opportunity for continuous variation of material parameters. Because the chalcogenides are good glass formers over such a wide range of alloy compositions, the discovery of PIRSH burning in this system presents the possibility of observing variations in hole burning behavior as the glass composition is varied in a systematic manner, thereby illuminating correlations between the hole burning behavior and other properties of the glass. Mapping out the spontaneous hole filling behavior as a function of composition could reveal, for example, whether the distribution of hole burning barriers evolves continuously, or whether there are abrupt phase transitions at certain compositions as might be expected if recent theories[40] of a rigidity percolation at certain atomic coordination numbers are correct.

As we have seen, substantial variations in the temperature-dependent dephasing processes also exist among the various chalcogenide hosts. The problem of optical dephasing in glasses has drawn much attention[41] ever since it was first discovered[42,43] that homogeneous linewidths for rare earth ions in inorganic glasses at low temperatures are much larger and follow very different temperature dependences than those for the same impurities in crystalline hosts. While dephasing in crystals at low temperature is dominated by scattering of acoustic phonons (phonon Raman processes), yielding linewidths which increase as T^7 for temperatures below the Debye temperature, and as T^2 above the Debye temperature,[44] these early results for inorganic glasses, in contrast, displayed T^2 behavior down to the lowest temperatures. The picture grew more complex as new experimental results revealed temperature dependences below ~10 K varying from $T^{1.0}$ to $T^{2.2}$ for a wide range of impurities in both organic and inorganic systems, with little apparent pattern to these results, except possibly for a rough tendency for organic systems to fall near $T^{1.3}$ and for inorganic systems to fall near T^2.

No single theory of dephasing in glasses has yet emerged which satisfactorily explains all of the experimental results. The standard model used in most theories

assumes that low temperature dephasing is due to the same entities originally proposed in the tunneling model for the low temperature specific heat of glasses.[23,24] Recall that in the tunneling model, the glass may be described by a collection of double-well potentials with groups of glass atoms tunneling between two configurations, i.e. as a collection of two-level systems (TLS) . In order to account for the linear term in the low temperature specific heat, the density of states as a function of tunneling energy for the TLSs is assumed to be constant. Most theories of optical dephasing envision the defect coupled to a sea of TLSs which modulate the energy levels of the defect. The TLSs are in turn coupled to phonons which can induce transitions between the TLS levels. The resulting temperature dependence of the linewidth will then depend on the TLS density of states and the form of the coupling between the defect and TLS (dipole-dipole, dipole-quadrupole, etc.), and is, unfortunately, very sensitive to the approximations made in performing the integral over all TLSs. These theories, with the appropriate initial assumptions, can all reproduce the "universal" $T^{1.3}$ behavior, but the assumptions vary considerably and tend to lack experimental justification. The T^2 behavior observed in many systems does not appear to be satisfactorily explained by theories of this kind; it has been suggested[45] that the high T regime of phonon Raman dephasing may extend to lower temperatures in glasses due to highly non-Debye densities of states. Besides the standard TLS models, other theories, involving "fractons"[46] and "tunnelons"[47] have also been proposed to explain dephasing processes in glasses. Since a complete discussion of current theories is beyond the scope of the present article, the reader is referred to any of the several reviews of the subject for more details.[5,41,48]

Clearly more work is needed in order to construct a coherent picture of optical dephasing in glasses. Part of the problem on the experimental side has been that, despite the relatively large number of systems studied so far, these systems have tended to be unrelated, so that too many parameters change in going from one system to another to ascertain which properties are important in determining, for instance, why some systems show $T^{1.3}$ dephasing behavior while others show T^2. As we have seen in the few examples presented here, the chalcogenide glasses display virtually the entire range of temperature dependences observed for optical linewidths in glasses. The $T^{1.27}$ behavior seen in *a*-Se is similar to that of many organic systems while the $\sim T^2$ behavior of As_2S_3 is reminiscent of the early results for inorganic glasses. Thus, with the continuous variability of alloy composition possible with chalcogenide glasses, is should now be possible to obtain correlations between the dephasing behavior and other glass parameters such as the glass transition temperature, elastic constants, microscopic structure, and average atomic coordination number, all of which may be varied simply by changing the alloy composition. The information gained by such a systematic study may help unravel some of the current confusion surrounding the anomalous optical dephasing in amorphous materials, and provide the basis for futher theoretical work on the nature of low energy excitations in glasses.

ACKNOWLEDGEMENTS

The authors would like to thank W. P. Ambrose and J. P. Sethna for valuable discussions during the course of this work. This work was supported by the National Science Foundation grant DMR-87-14600, and by the U. S. Army Research Office grant DAAL03-86-0103.

REFERENCES

1. P. H. Lee and L. S. Skolnick, Appl. Phys. Lett. **10**, 303 (1967).

2. A. Szabo, Phys. Rev. B **11**, 4512 (1975)

3. A. A. Gorokhovskii, R. K. Kaarli, and L. A. Rebane, JETP Lett. **20**, 216 (1974).

4. B. M. Kharlamov, R. I. Personov, and L. A. Bykovskaya, Opt. Commun. **12**, 191 (1974).

5. J. M. Hayes, R. Jankowiak, and G. J. Small in *Persistent Spectral Hole Burning: Science and Applications*, W. E. Moerner, ed. (Springer-Verlag, Berlin 1988), Chapter 5.

6. R. M. Macfarlane and R. M. Shelby in *Persistent Spectral Hole Burning: Science and Applications*, W. E. Moerner, ed. (Springer-Verlag, Berlin 1988), Chapter 4.

7. For a review see A. J. Sievers and W. E. Moerner in *Persistent Spectral Hole Burning: Science and Applications*, W. E. Moerner, ed. (Springer-Verlag, Berlin 1988), Chapter 6.

8. M. Dubs and H. H. Günthard, Chem. Phys. Lett. **64**, 105 (1979).

9. M. Dubs and H. H. Günthard, J. Mol Struct. **60**, 311 (1980).

10. M. Dubs, L. Ermanni, and H. H. Günthard, J. Mol. Spectry. **91**, 458 (1982).

11. W. E. Moerner, A. J. Sievers, R. H. Silsbee, A. R. Chraplyvy, and D. K. Lambert, Phys. Rev. Lett. **49**, 398 (1982).

12. W. E. Moerner, A. R. Chraplyvy, A. J. Sievers and R. H. Silsbee, Phys. Rev. B **28**, 7244 (1983).

13. W. E. Moerner, A. R. Chraplyvy, A. J. Sievers and R. H. Silsbee, Phys. Rev. B **29**, 4791 (1984).

14. R. C. Spitzer, W. P. Ambrose and A. J. Sievers, Opt. Lett. **11**, 428 (1986).

15. R. C. Spitzer, W. P. Ambrose and A. J. Sievers, Phys. Rev. B **34**, 7307 (1986).

16. W. P. Ambrose and A. J. Sievers, Chem. Phys. Lett. **147**, 608 (1988).

17. W. P. Ambrose and A. J. Sievers, Phys. Rev. B **38**, 10170 (1988).

18. S. P. Love and A. J. Sievers, Chem. Phys. Lett. **153**, 379 (1988).

19. S. P. Love and A. J. Sievers, Bull. Am. Phys. Soc. **33**, 784 (1988).

20. S. P. Love and A. J. Sievers, *Proceedings of the 7th International Conference on Dynamical Processes in Excited States of Solids*, J. Luminescence (1989).

21. R. Frerichs, J. Opt. Soc. Am. **43**, 1153 (1953).

22. For a proper density-matrix treatment of the problem of optical absorption by ensembles of molecules see R. L. Shoemaker in *Laser and Coherence Spectroscopy*, J. L. Steinfeld, ed. (Plenum Press, New York, 1978), p. 197.

23. P. W. Anderson , B. I. Halperin, and C. M. Varma, Philos. Mag. **25**, 1 (1971).

24. W. A. Phillips, J. Low Temp. Phys. **7**, 351 (1972).

25. R. T. Harley, M.J. Henderson, and R. M. Macfarlane, J. Phys. C **17**, L233 (1984).

26. S. P. Love, K. Muro, R. E. Peale, A. J. Sievers and W. Lo, Phys. Rev. B **36**, 2950 (1987).

27. D. Haarer in *Persistent Spectral Hole Burning: Science and Applications*, W. E. Moerner, ed. (Springer-Verlag, Berlin 1988), Chapter 3.

28. K. K. Rebane and L. A. Rebane in *Persistent Spectral Hole Burning: Science and Applications*, W. E. Moerner, ed. (Springer-Verlag, Berlin 1988), Chapter 2.

29. S. Völker, J. Luminescence **36**, 251 (1987).

30. M. Berg, C. A. Walsh, L. R. Narasimhan, K. A. Littau, and M. D. Fayer, J. Chem. Phys. **88**, 1564 (1988).

31. For a review of photon echo and other coherent optical transient techniques, see M. D. Levenson, *Introduction to Nonlinear Laser Spectroscopy* (Academic Press, New York, 1982).

32. C. H. Henry and R. F. Kazarinov, IEEE J. Quant. Electronics **QE-22**, 294 (1986).

33. L. S. Rothman and W. S. Benedict, Appl. Opt. **17**, 2605 (1978).

34. P. F. Bernath, T. Amano, and M. Wong, J. Mol. Spectry. **98**, 20 (1983).

35. W. Rohrbeck, A. Hinz, and W. Urban, Mol. Phys. **41**, 925 (1980).

36. R. S. Lowe, Mol. Phys. **41**, 929 (1980).

37. K. Nakamoto, *Infrared and Raman Spectra of Inorganic and Coordination Compounds*, third edition, (Wiley, New York, 1978).

38. R. Jankowiak, R. Richert, and H. Bässler, J. Phys. Chem. **89**, 4569 (1985).

39. R. Jankowiak, L. Shu, M. J. Kenney and G. J. Small, J. Luminescence **36**, 293 (1987).

40. H. He and M. F. Thorpe, Phys. Rev. Lett. **54**, 2107 (1985).

41. For many excellent reviews, see *Optical Linewidths in Glasses*, M. J. Weber, ed., J. Luminescence **36**, 179-329 (1987).

42. P. M. Selzer, D. L. Huber, D. S. Hamilton, W. M. Yen, and M. J. Weber, Phys. Rev. Lett. **36**, 813 (1976).

43. J. Hegarty and W. M. Yen, Phys. Rev. Lett. **43**, 1126 (1979).

44. B. DiBartolo, *Optical Interactions in Solids*, (Wiley, New York, 1968).

45. D. L. Huber, J. Non-Cryst. Solids **51**, 241 (1982).

46. S. K. Lyo and R. Orbach, Phys. Rev. B **29**, 2300 (1984).

47. I. S. Osad'ko and A. A. Shtygashev, J. Luminescence **36**, 315 (1987).

48. R. Silbey and K. Kassner, J. Luminescence **36**, 283 (1987).